Protist 179 (2025) 126120

Contents lists available at ScienceDirect

Protist

journal homepage: www.elsevier.de/protis

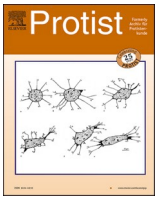

Diversity of *Kryptoperidinium* (Peridiniales, Dinophyceae): Morphological description and molecular phylogenetics of *Kryptoperidinium secundum* sp. nov.

Urban Tillmann [a,*], Marc Gottschling [b], Stephan Wietkamp [a], Ilka Peeken [a], Jennifer Wolny [c], Norico Yamada [d,1]

[a] *Alfred-Wegener-Institute, Helmholtz Centre for Polar and Marine Research, Am Handelshafen 12, D – 27570 Bremerhaven, Germany*
[b] *Fakultät für Biologie – Systematik, Biodiversität & Evolution der Pflanzen, GeoBio-Center, Ludwig-Maximilians-Universität München, Menzinger Str. 67, D – 80638 München, Germany*
[c] *Office of Applied Microbiology and Technology, Human Foods Program, US Food and Drug Administration, College Park, MD 20740, USA*
[d] *Department of Natural History Sciences, Graduate School of Science, Hokkaido University, Kita-10 Nishi-8, Kita-Ku, Sapporo 0600810, Japan*

ARTICLE INFO

Keywords:
Co-divergence
Dinoflagellate
Dinotom
Molecular phylogenetics
Morphology
New World
Taxonomy

ABSTRACT

Kryptoperidinium belongs to a group of dinophytes hosting a diatom as an endosymbiont and is currently considered to comprise a single, putatively bloom-forming and harmful species only. Molecular phylogenetics indicate the existence of a second distinct lineage and therefore species new to science, which we here formally describe as *Kryptoperidinium secundum* sp. nov. We studied living and fixed material of unialgal strains in detail using light and electron microscopy and gained DNA sequences of the rRNA complex (hosts and endosymbionts, from which also *psb*A and *rbc*L sequence data were obtained). In a molecular phylogeny of the Bacillariophyceae, the endosymbionts of *K. secundum* have a divergent position from those of *Kryptoperidinium triquetrum* (=*K. foliaceum*) and show (once more) a close relationship to free-living diatoms. The cells of *K. secundum* were strongly dorso-ventrally compressed and exhibited the thecal plate formula po, X, 4′, 2a, 7″, 5C, 6(?)S, 5‴, 2⁗. The distalmost precingular plate was consistently rectangular in shape and relatively broad, and this is the key diagnostic trait to distinguish *K. secundum* from the known *K. triquetrum*, which has a characteristically L-shaped plate with a thin and elongated base. The two species are clearly divergent in molecular phylogenetics (exhibiting long branches) and constitute a monophyletic group together with *Dinothrix* sharing the same thecal plate formula. The diatom phylogeny favours an evolutionary scenario of repeated plastid capture rather than strict co-divergence between dinophyte hosts and their endosymbionts.

1. Introduction

Kryptoperidiniaceae are a monophyletic group of unicellular dinophytes hosting diatoms as endosymbiont (Tomas et al., 1973; Horiguchi, 2004) and are colloquially termed ‘dinotoms’. They comprise some 25 species of *Blixaea* Gottschling, *Dinothrix* Pascher, *Durinskia* Carty & El.R. Cox, *Kryptoperidinium* Er.Lindemann and *Unruhdinium* Gottschling occurring in both marine and freshwater environments (Gottschling, 2017; Moestrup and Calado, 2018; Yamada et al., 2020; Baharudin et al., 2025). The endosymbiosis between the diatom and the dinophyte host is considered obligate for most species, but the degree of evolutionary co-divergence has been shown to be limited indicating a repeated capture of the endosymbiont (Žerdoner Čalasan et al., 2018; Tillmann et al., 2023). No reliable fossils of the group are known, but Kryptoperidiniaceae appear geologically old and have been consistently dated to the Cretaceous by molecular clock analyses (Žerdoner Čalasan et al., 2019; Chacón and Gottschling, 2020). This is remarkable given the modest size of the species group and the early evolutionary stage of plastid integration, in which Kryptoperidiniaceae may reside (Tillmann et al., 2023).

Among dinotoms, *Kryptoperidinium* is best studied and most widespread and is easy to identify because of the cell’s strong dorso-ventral compression (Lindemann, 1924). It has been reported worldwide from the Atlantic Ocean (Paulsen, 1908; Lebour, 1925; Kempton et al., 2002;

* Corresponding author.
E-mail address: urban.tillmann@awi.de (U. Tillmann).
[1] Present address: Station Biologique de Roscoff, French National Center for Scientific Research, Place Georges Teissier, F – 29680, Roscoff, France.

https://doi.org/10.1016/j.protis.2025.126120
Received 16 May 2025; Accepted 27 August 2025
Available online 28 August 2025

Wolny et al., 2022), the North Sea (van Goor, 1925), the Baltic Sea (Lindemann, 1924), the Mediterranean Sea (Biecheler, 1952; Satta et al., 2020), the Black Sea (Krakhmalny et al., 2018), the Caspian Sea (Lewis et al., 2018), the Red Sea (Alkawri, 2016), the Indian Ocean (Arabian Gulf: Saburova et al., 2012b), Australia (Hallegraeff et al., 2010) and the Pacific Ocean (Costa Rica: Dodge and Crawford, 1969). Moreover, the algae have been investigated in detail regarding life history (Silva, 1962; Figueroa et al., 2009), behaviour (Moldrup and Garm, 2012), ultrastructure (Dodge and Crawford, 1969; Bricheux et al., 1992), composition of lipid globules (Withers and Haxo, 1978), physiology and nutrition (Droop, 1958; Prager, 1963) and pigment profiles (Kempton et al., 2002; Zapata et al., 2012).

Kryptoperidinium is commonly found in coastal waters such as estuaries, lagoons and tidal creeks and is reported to occur in a very wide range of environmental conditions. The algae have been detected at salinities ranging from almost freshwater (salinity <0.5) in inner areas of the Spanish Guirdina estuary (Domingues et al., 2011) to hypersaline habitats (salinity >100) of the Arabian Gulf (Saburova et al., 2012b) and at water temperatures ranging from 10 °C (Silva, 1962) to 34 °C (Alkawri, 2016). *Kryptoperidinium* can dominate plankton communities in dense blooms (Lindemann, 1924; Lebour, 1925; van Goor, 1925; Grøntved, 1950; Silva, 1962; Prager, 1963; Pybus et al., 1984; Wolny et al., 2004; Turki et al., 2007; Alkawri, 2016) with maximal densities of up to 4.8 million cells per litre (Silva, 1962). Such blooms have been linked to fish kills (Lindemann, 1924; Turki et al., 2007) or associated with shellfish mortality (Kempton et al., 2002; Wolny et al., 2004).

Currently, *Kryptoperidinium* is considered monospecific, and the application of the species' name was confusing (Gottschling et al., 2018). For a long time, the name *Kryptoperidinium* (≡ *Peridinium*) *foliaceum* (F.Stein) Er.Lindemann was applied, but this is a younger heterotypic synonym of, and is nomenclaturally replaced today by, *Kryptoperidinium triquetrum* (Ehrenberg) Tillmann, Gottschling, Kusber, Hoppenrath & Elbrächter (Gottschling et al., 2019). Notably, both such species names have been described based on material from the Baltic Sea off Wismar and are now taxonomically clarified by epitypification (Tillmann et al., 2023), making *K. triquetrum* the accepted name. Previous considerations of globally collected strains already have indicated that *Kryptoperidinium* may comprise of an additional species (Kempton et al., 2002; Wolny et al., 2004). Molecular DNA sequence data of the ribosomal RNA (rRNA) complex, which includes SSU, ITS and LSU gene regions, retrieve two lineages, one of which is unambiguously identified as *K. triquetrum* (Tillmann et al., 2023). However, the second lineage cannot be provided with a scientific name at this moment in time, and a critical morphological inspection is lacking as well.

Details on the morphology of *Kryptoperidinium* in the literature are not always consistent, and there are, for example, deviating reports with respect to the presence or absence of the eye spot (Saburova et al., 2012b). Similarly, the endosymbiont nucleus has not been detected in all previous studies (Kempton et al., 2002). The thecal plate formula of *Kryptoperidinium* may comprise either three (Figueroa et al., 2009) or four apical plates (Kempton et al., 2002; Saburova et al., 2012b; Satta et al., 2020), and the number of cingular plates is also unclear (Kempton et al., 2002; Figueroa et al., 2009). However, most studies lack accompanying molecular data, and it is challenging to evaluate whether morphological deviations are due to wrong observations or aged strains or are in fact reflecting reproductive isolation between different species of *Kryptoperidinium*.

In this study, we investigate the biodiversity of *Kryptoperidinium*. We focus on a hitherto poorly understood, second evolutionary lineage that exists in addition to the established *K. triquetrum* (= *K. foliaceum*) and that we name *Kryptoperidinium secundum* sp. nov. We study several strains using a plethora of light and electron microscopic methods and compare the morphological variability with phylogenetic trees of the hosts and their endosymbionts generated on the basis of concatenated rRNA sequences. In this way, we aim at contributing to a better knowledge of an ecologically important group of dinophytes that may pose a threat through bloom formation and toxin production.

2. Materials and Methods

2.1. Strain cultivation

As part of a broader study on the morphology and phylogeny of *Kryptoperidinium*, two strains for which no molecular or morphological data had previously been available were selected for detailed investigation. These two strains (ARC121 and ARC231) were obtained from the Algal Resources Collection (ARC). Both strains were collected from the Neuse River (USA–NC) in 2008. They were grown at 15 °C under a photon flux density of 80 µmol m^{-2} s^{-1} on a 16:8 h light:dark photocycle in a natural seawater medium consisting of sterile filtered (0.2 µm VacuCap filters, Pall Life Sciences, Dreieich, Germany) and North Sea water diluted to a salinity of 20. Nutrients were added corresponding to 50 % of K-medium (Keller et al., 1987), which was slightly modified by replacing the organic phosphorous source with 3.62 µM Na_2HPO_4.

For DNA harvest, cells were collected by centrifugation (Eppendorf 5810R; Hamburg, Germany) in 50 mL centrifugation tubes at 3220 ×*g* for 10 min. Cell pellets were transferred with 0.5 mL lysis buffer (SL1, provided by the NucleoSpin Soil DNA extraction Kit of Macherey-Nagel; Düren, Germany) to 1 mL microtubes and stored frozen (−20 °C) for subsequent DNA extraction.

2.2. Microscopy

Observation of living or fixed cells (formaldehyde: 1 % final concentration, or neutral Lugol-fixed: 1 % final concentration) was carried out using an inverted microscope (Axiovert 200 M: Zeiss; Munich, Germany) and a compound microscope (Axiovert 2: Zeiss), both equipped with epifluorescence and differential interference contrast optics. Living cells were recorded using a digital video camera (Gryphax, Jenoptik; Jena, Germany) at full-HD resolution. Single frame micrographs were extracted using Corel Video Studio software (Version X8 pro: Corel; Ottawa, Canada). Images of fixed cells were taken with a digital camera (Axiocam MRc5: Zeiss).

Light microscopic (LM) examination of thecal plates was performed on fixed cells (neutral Lugol) stained with Solophenyl Flavine (Carbosynth; Compton, US–CA), a fluorescent dye specific to cellulose. Epifluorescence microscopy was used to determine the shape and location of the nucleus (UV excitation, filter set 01; Zeiss) after staining of formalin-fixed cells with 4′,6-diamidino-2-phenylindole (DAPI, 0.1 µg mL^{-1} final concentration) for 10 min. Cell length and width were measured at 1000× microscopic magnification using freshly fixed cells (formaldehyde, 1 % final concentration) from dense strains at late exponential growth phase (based on stereomicroscopic inspection of the living material) and the Axiovision software (Zeiss).

For scanning electron microscopy (SEM), Lugol-fixed cells were collected by gentle filtration on 3 µm pore-size polycarbonate filters and were subsequently processed for SEM (FEI Quanta FEG 200; Eindhoven, the Netherlands) as described previously (Tillmann et al., 2023).

2.3. Pigment analyses

For pigment analysis with HPLC (high performance liquid chromatography), various strains of *Kryptoperidinium* (Table 1) were grown in 65 mL plastic culture flasks at the culture conditions described above. During exponential growth phase at cell densities between 0.5 and 3.6 × 10^3 cell mL^{-1} (as estimated by microscopic cell counts), 30–50 mL were gently filtered on to a glass-fibre filter (25 mm Ø, GF/C, Whatman, Kent, UK–England). Filters were immediately flash frozen in liquid nitrogen and stored at −80 °C.

Pigments were measured and quantified with a Waters Alliance 2695 HPLC Separation Module connected to a Waters photodiode array detector (2996). The filters were extracted in 100 % acetone HPLC grade

Table 1
Strains of *Kryptoperidinium* used for pigment analyses. Strains ARC121 and ARC231 were provided by the Algal Resources Collection (ARC). Strain KFF 1001 was obtained from the FINMARI Culture collection/SYKE Marine Research Centre and Tvärminne Zoological Station (FINMARI CC).

Species	Strain	Isol. year	Origin
K. secundum	ARC121	2008	USA–NC: Neuse River
K. secundum	ARC231	2008	USA–NC: Neuse River
K. triquetrum	W1-E4	2019	Baltic Sea, off Germany: Wismar
K. triquetrum	W1-D8	2019	Baltic Sea, off Germany: Wismar
K. triquetrum	W1-D11	2019	Baltic Sea, off Germany: Wismar
K. triquetrum	W4-A6	2019	Baltic Sea, off Germany: Wismar
K. triquetrum	W4-F9	2019	Baltic Sea, off Germany: Wismar
K. triquetrum	G-E8	2019	Baltic Sea, off Germany: Greifswald
K. triquetrum	KFF 1001	2010	Baltic Sea, off Finland: Föglö
K. triquetrum	GeoB 459	2010	Mediterranean (Aegean) Sea, off Greece

and the samples were homogenised with small glass beads in a Precellys tissue homogeniser and thereafter centrifuged (0 °C). The supernatant liquid was filtered through a 0.2 µm PTFE filter (Rotilabo) and stored at −80 °C prior to analysis.

An aliquot of 120 µL was transferred to the auto sampler (4 °C). The auto sampler uses a step function to draw the liquid from the sample and 1 M ammonium acetate solution (4 × 25 µL each, prior to analysis), which is sufficient to serve as a mixing between the two solvents. The analysis of the pigments was conducted by reverse-phase HPLC using a Microsorb-MV3 C8 column (4.6 × 100 mm), and HPLC-grade solvents using a modified method of Barlow et al. (1997). The system was calibrated with standards from DHI, except for chlorophyll *c1* and γ-carotene (since no standards were available) and instead, the response factor of chlorophyll *c2* and ß-carotene were used for quantification.

2.4. Molecular phylogenetics

For species of *Kryptoperidinium*, genomic DNA of the studied material was extracted following the manufacturers' instructions of the NucleoSpin Soil DNA extraction Kit (Macherey-Nagel; Düren, Germany) with an additional cell disruption step within the beat tubes. The samples were shaken in a FastPrep FP120 cell disrupter (Qbiogene; Carlsbad, US–CA) for 45 s and another 30 s at a speed of 4.0 m s^{-1}. For the elution step, 50 µL of the provided elution buffer were spun through the column, and elution was subsequently repeated with another 50 µL to increase the DNA yield. For species of *Dinothrix*, genomic DNA extraction was performed using the QuickExtract FFPE RNA Extraction Kit (Epicentre; Madison, US–WI). For both hosts and endosymbionts, various regions of the rRNA compleex were amplified as outlined in Yamada et al. (2020) and Tillmann et al. (2023). Amplicon purification followed the instructions of the NucleoSpin Gel and PCR clean-up kit (Macherey-Nagel), and PCR products were sequenced directly in both directions on an ABI PRISM 3730XL (Applied Biosystems; Waltham, USA–MA) using the ABI Big-Dye dye-terminator technique (Applied Biosystems) accordingly to the manufacturer's recommendations.

Raw sequence data were processed using the CLC Genomics Workbench 12 (Qiagen; Hilden, Germany). Sequences were edited and assembled using Sequencher™v5.1 (Gene Codes; Ann Arbor, USA–MI). For visual comparison of the edited sequences, the alignment editor 'Se-Al' (http://tree.bio.ed.ac.uk/software/seal/) was used. Molecular phylogenetics of both dinophyte hosts and diatom endosymbiont were performed as described previously (Tillmann et al., 2023), and all sequences used were compiled in the Voucher List (Table S1). In order to utilise the full power of phylogenetic information from rRNA sequences, we followed a concatenation approach, which provides higher-quality results than single-gene analyses. Alignments were built with the help of MAFFT v6.502a (Katoh and Standley, 2013) and are available upon request. Phylogenetic analyses were carried out by using Maximum Likelihood (RAxML v8.2.12: Stamatakis, 2014) and Bayesian sofware (MrBayes v3.2.7a: Ronquist et al., 2012).

3. Results

3.1. General morphology

Both strains ARC121 and ARC231 were morphologically indistinguishable. From strain ARC121, the holotype of *K. secundum* sp. nov. was prepared, and this strain will be described and depicted in detail. Additional micrographs of strain ARC231 are available as Supplementary Material. The strains exhibited predominantly flagellated, motile cells and occasionally deflagellated, immotile cells at the bottom of the cultivation vessels.

The motile cells (Fig. 1A–R) varied in size (Fig. 1), and cell length ranged from 17.5 to 37.4 µm without forming distinct size classes. They were variable in the length/width ratio (range: 0.76–1.19) with a mean value (1.07 ± 0.07, $n = 49$) only slightly larger than 1. Cell depth (in lateral view) was difficult to measure but comprised ca 50 % of the cell's length (Fig. 1E, F, I). The cells were equipped with a transverse flagellum and a longitudinal flagellum, which were about the length of the cell. Cells swam with rapid turns in narrow, helical paths (Suppl. Video SV01). Exponentially growing cultures had an intensely yellow to orange-brown colour (Fig. 1A–R).

In ventral view, cells were slightly variable in outline with an asymmetrically rounded episome and with a rather symmetric and rounded hyposome (Fig. 1A, G, M–R). They were dorso-ventrally compressed with dorsally convex and ventrally concave surfaces (Fig. 1D–F, I). The cingulum was narrow (ca 1.4 µm in height), excavated and almost had a median or slightly sub-median position. As a result, the episome was only slightly larger than the hyposome, if at all. The cingular groove was discontinuous in the ventral area, and there was only slight and descending cingular displacement. Just below the cingulum, the sulcal area formed a narrow and closed funnel (arrow in Fig. 1M) for the longitudinal flagellum.

A number of globular to ovoid or slightly elongated, small plastids were peripherally located (Fig. 1A–R). Brightfield microscopy of living cells revealed a large, ovoid nucleus located in the cingular area on the cell's left-lateral site (Fig. 1R). However, it was difficult to observe, as it mostly was obscured by the densely packed plastids. Chromatin staining and fluorescence microscopy (Fig. 1S, T) clearly showed the presence of two nuclei, including the large dinophyte nucleus with condensed chromosomes. Additionally, the nucleus of the endosymbiont was highly irregular in shape and more faintly stained, and no chromosomes were discernible. In the central sulcal area just below the cingulum and extending onto the hyposome, a conspicuous eyespot of intense red colour was present. It had a very characteristic, rectangular or trapezoid shape with a slightly acuminate posterior part and a hook-shaped anterior projection (Fig. 1O, Q). In stationary growth phase, cells accumulated clumps of light or dark brown globules in the centre (Fig. 1U–X).

In cultures, during exponential growth, dividing and pre-division cells were easily distinguishable on the bottom of the vessels and were immotile and spherical (Fig. 2A–J). From these sporocysts, two (Fig. 2 E, H–J) or four flagellated daughter cells (Fig. 2G) hatched and left behind the thin, hyaline envelope of the pellicle (Fig. 2J). Occasionally, only a solitary cell eclosed from the pellicle (Suppl. Video SV01). Sometimes, larger numbers of small cells were observed (Fig. 2K, L) swarming around each other with high speed in close circles with repeated cell-to-cell contact events (Suppl. Video SV01). Pairing cells (Fig. 2M–S) were attached to each other at different angles in their sulcal regions.

3.2. Thecal plate pattern

The thecal plate pattern of living cells was faintly visible in light microscopy, but could be elucidated with epifluorescence microscopy after cellulose staining (Fig. 3). This was confirmed and supplemented

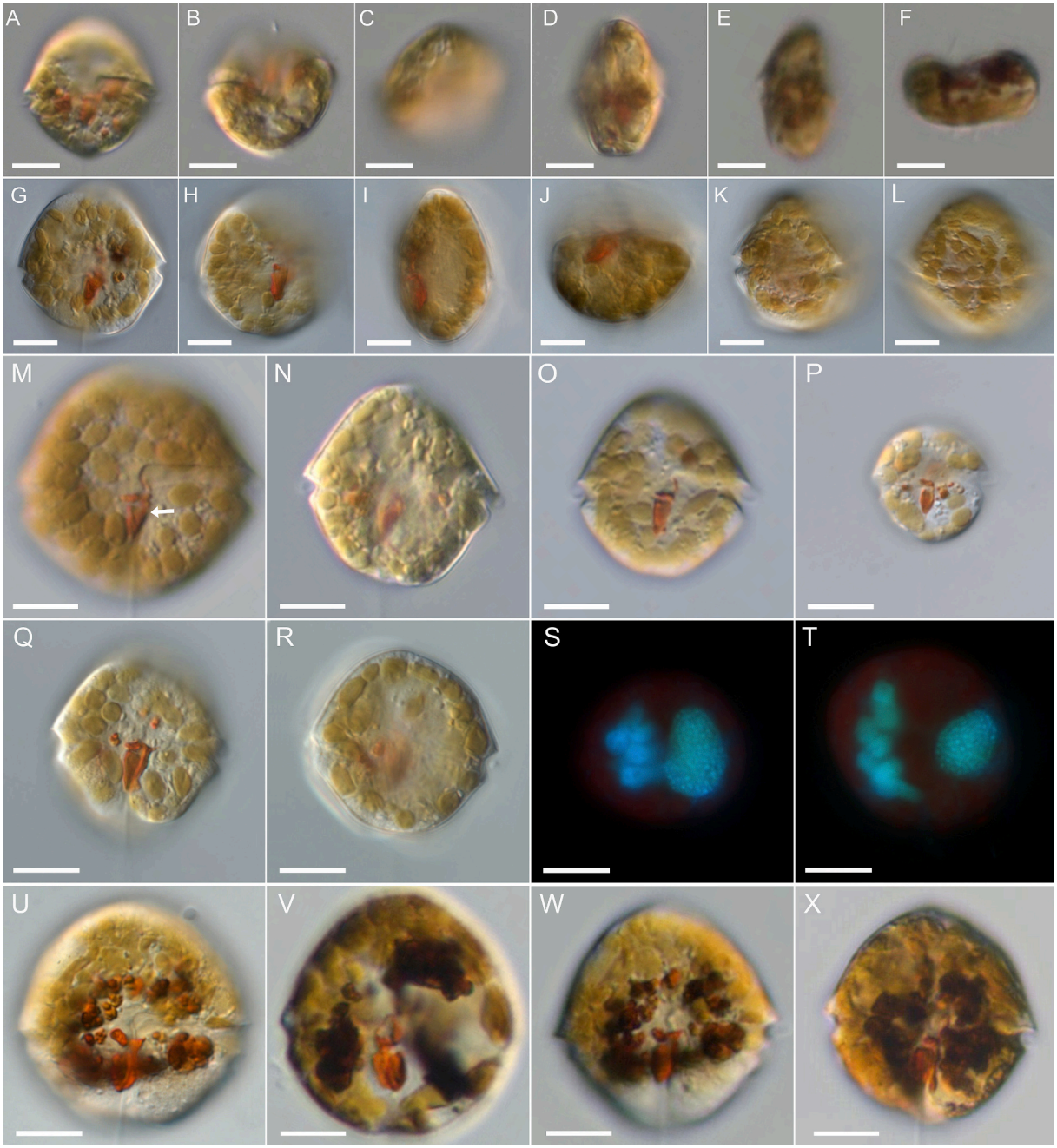

Fig. 1. *Kryptoperidinium secundum*, strain ARC121. Light microscopy of living cells (A–R; U–X) or formalin-fixed cells (S, T). (A–D) The same cell in ventral (A), ventral-antapical (B), ventral-apical (C), lateral view (D). (E, F) Another cell in lateral (E), antapical view (F). (G–J) Another cell in ventral (G), ventral-lateral (H), lateral (I), antapical view (J). (K, L) Another cell in lateral (K), dorsal view (L). (M–P) Cells of different size in ventral view. (Q, R) Two different focal planes of the same cell in ventral view. (S, T) Different cells stained with DAPI and viewed with epifluorescence and UV excitation. Note the irregularly shaped diatom nucleus (left) and the dinophyte nucleus with condensed chromosomes (right). (U–X) Different cells in stationary growth phase with light or dark brown globules accumulating in the cell centre. Scale bars: 10 μm. (For interpretation of the references to colour in this figure legend, the reader is referred to the web version of this article.)

by SEM analyses (Fig. 4). Thecal plates were smooth but densely ornamented with small pores, which were mostly scattered over the ventral plates (Figs. 3A–D, 4A). Only occasionally, the pores were arranged in rows on some dorsal plates of the epitheca (Figs. 3H, 4C). The plate pattern was identified as po, X, 4′, 2a, 7″, 5C, 6(?)S, 5‴, 2⁗ and is schematically drawn in Fig. 5.

In the apical position of the epitheca, there was a slender and elongated pore plate with a slender apical pore opening (Fig. 3A, B, G). Ventrally to the pore plate, a small X-plate (canal plate) was present, which was rectangular, longer than wide and often asymmetrically tapered at the posterior end (Fig. 3A–D, 4E). In the ventral centre of the epitheca, there was a large plate with an inclined and straight or slightly curved suture towards its anteriorly adjacent plate (Fig. 3A–D, 4). Both plates corresponded to plate 1′, which was subdivided into an anterior part (here labelled as 1′ a) and a posterior part (here labelled as 1′ p). Plate 1′ a abutted the X-plate but not the pore plate. Plate 1′ p was in contact with both terminal cingular plates (i.e., C1 and C5) and both terminal precingular plates (i.e., 1″ and 7″: Fig. 3A–D, 4A). The second apical plate was located on the ventral side and had a very narrow contact to the pore plate (Fig. 3A, B). Plates 2′ and 3′ were of similar size

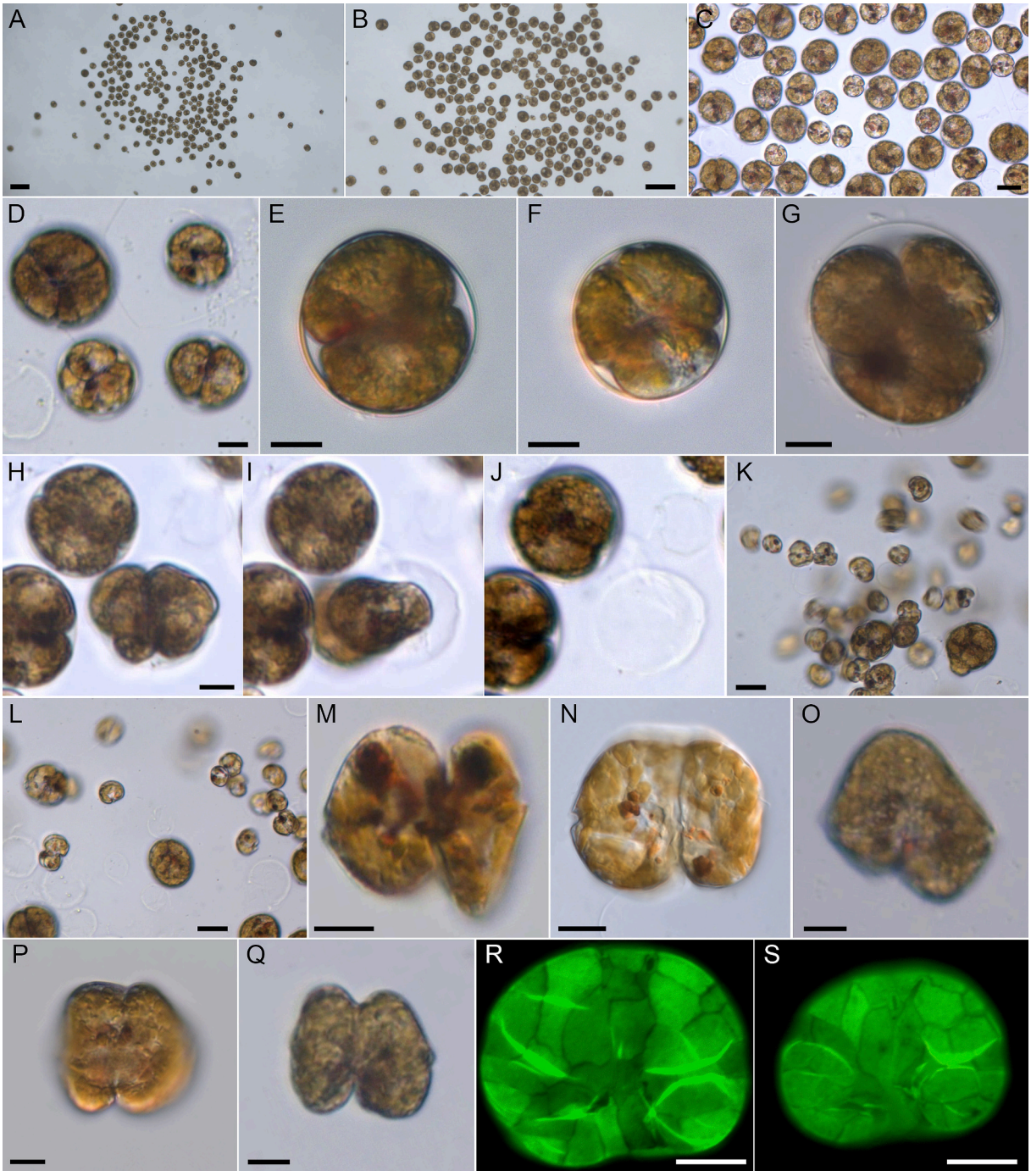

Fig. 2. *Kryptoperidinium secundum*, strain ARC121. Light microscopy of living cells (A–Q) or Lugol-fixed cells (R, S). (A–D) Deflagellated sporocysts accumulated at the bottom of the culture flask. (E) Sporocyst with two daughter cells. (F, G) Two differently sized sporocysts with four daughter cells. (H–J) Time series of two cells hatching. Note the empty pellicle left behind. (K, L) Agglomerations of small swarmer cells. (M–S) Different pairs of cells attached at different angles in their sulcal regions. (M–Q) Living cells. (R, S). Lugol-fixed cells stained with Solophenyl Flavine and viewed with epifluorescence and green light excitation. Scale bars: 100 µm (A, B), 20 µm (C, K, L), 10 µm (D–J, M–S). (For interpretation of the references to colour in this figure legend, the reader is referred to the web version of this article.)

but were smaller than the right-lateral plate 4′ (Fig. 3B, D, E, G).

There were two dorsally located anterior intercalary plates, of which plate 2a was slightly larger than plate 1a (Figs. 3E–H, 4B). Both intercalary plates were adjacent to six other epithecal plates. Among the series of seven precingular plates, plates 1″ to 5″ were of similar height, but the right-lateral and ventral plates 6″ and 7″ were taller (Fig. 3G, H). Plate 7″ was rectangular, longer than broad (Fig. 3A–D, 4), often had a slightly expanded base and shared a curved suture with plate 1′ p (Fig. 3B). The cingular groove was discontinuous and disconnected ventrally by plate 1′ p (Fig. 3A–D, 4). Plate C1 was smaller than the other cingular plates (Fig. 3A–F, 4A, B) although occasionally, plate C2 was of similar size as plate C1 (Fig. 3C). The suture between plates C2 and C3 (Fig. 3A–C) was in lateral position and thus often difficult to observe.

The hypotheca consisted of five postcingular plates and two antapical plates (Fig. 3A–J). The third postcingular plate was in dorsal position and adjacent to both antapical plates (Fig. 3E, F, H), which were of comparable sizes (Fig. 3J). The sulcal area was dominated by a longitudinal row of two large plates (Fig. 3K–M). The right sulcal plate (sd)

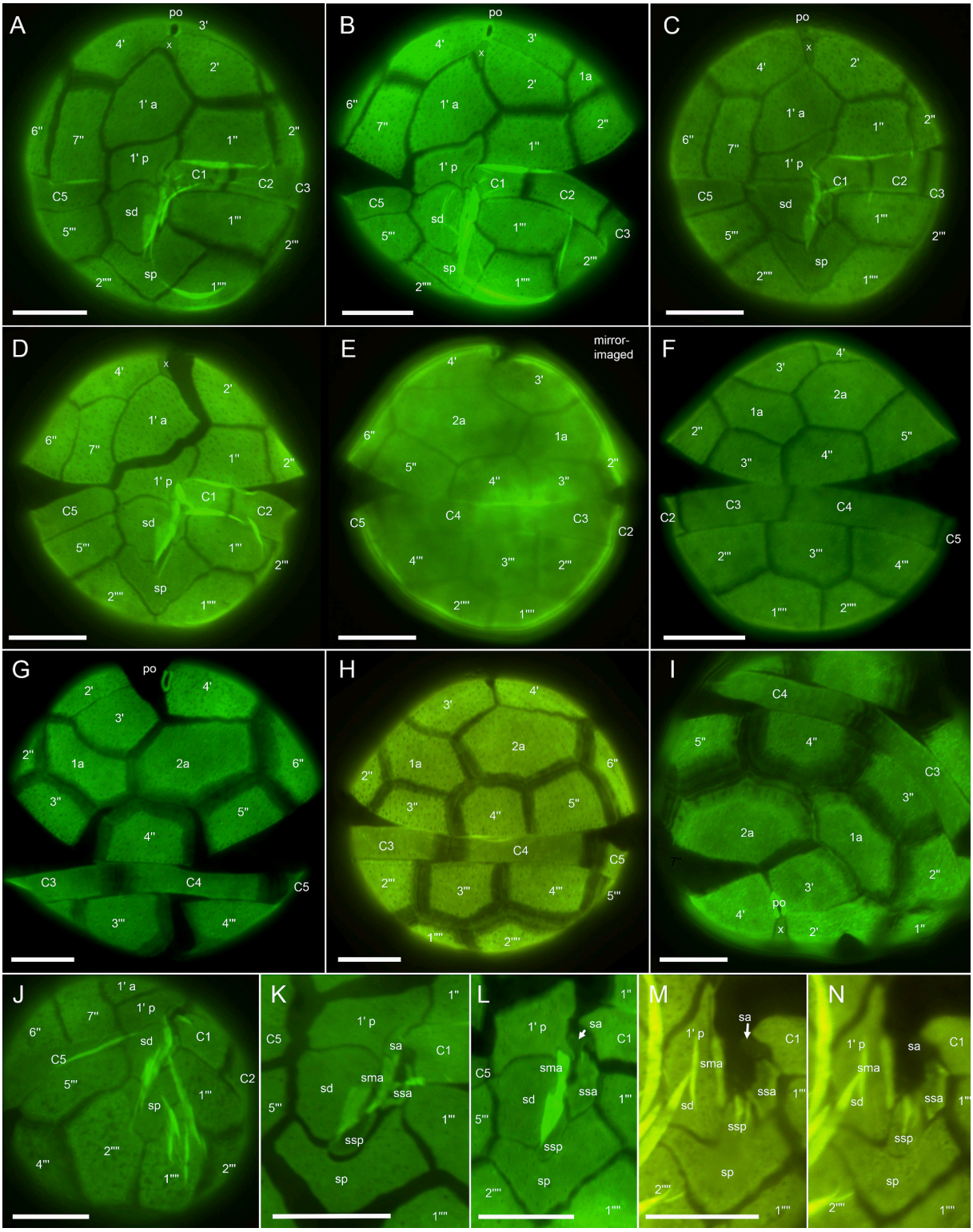

Fig. 3. *Kryptoperidinium secundum*, strain ARC121. Light microscopy of Lugol-fixed cells stained with Solophenyl Flavine and viewed with epifluorescence and green light excitation. (A–C) Cells in ventral view. (D, E) The same cell with focus on ventral (D) or dorsal (E) plates. Note that plate arrangement in E appears as mirror-imaged. (F–H) Cells in dorsal view. (I) Detailed view of epithecal plates in apical-dorsal view. (J) Detailed view of hypothecal plates in antapical-ventral view. (K–N) Detailed view of the sulcal area with sulcal plates. (M, N) Two different focal planes of the same cell. Plate labels according to the Kofoidean system, modified by labelling an anterior part (1' a) and a posterior part (1' p) of the first apical plate. Abbreviations: sa, anterior sulcal plate; sd, right sulcal plate; sma, anterior median sulcal plate; sp, posterior sulcal plate; ssa, anterior left sulcal plate; ssp, posterior left sulcal plate. Scale bars: 10 μm. (For interpretation of the references to colour in this figure legend, the reader is referred to the web version of this article.)

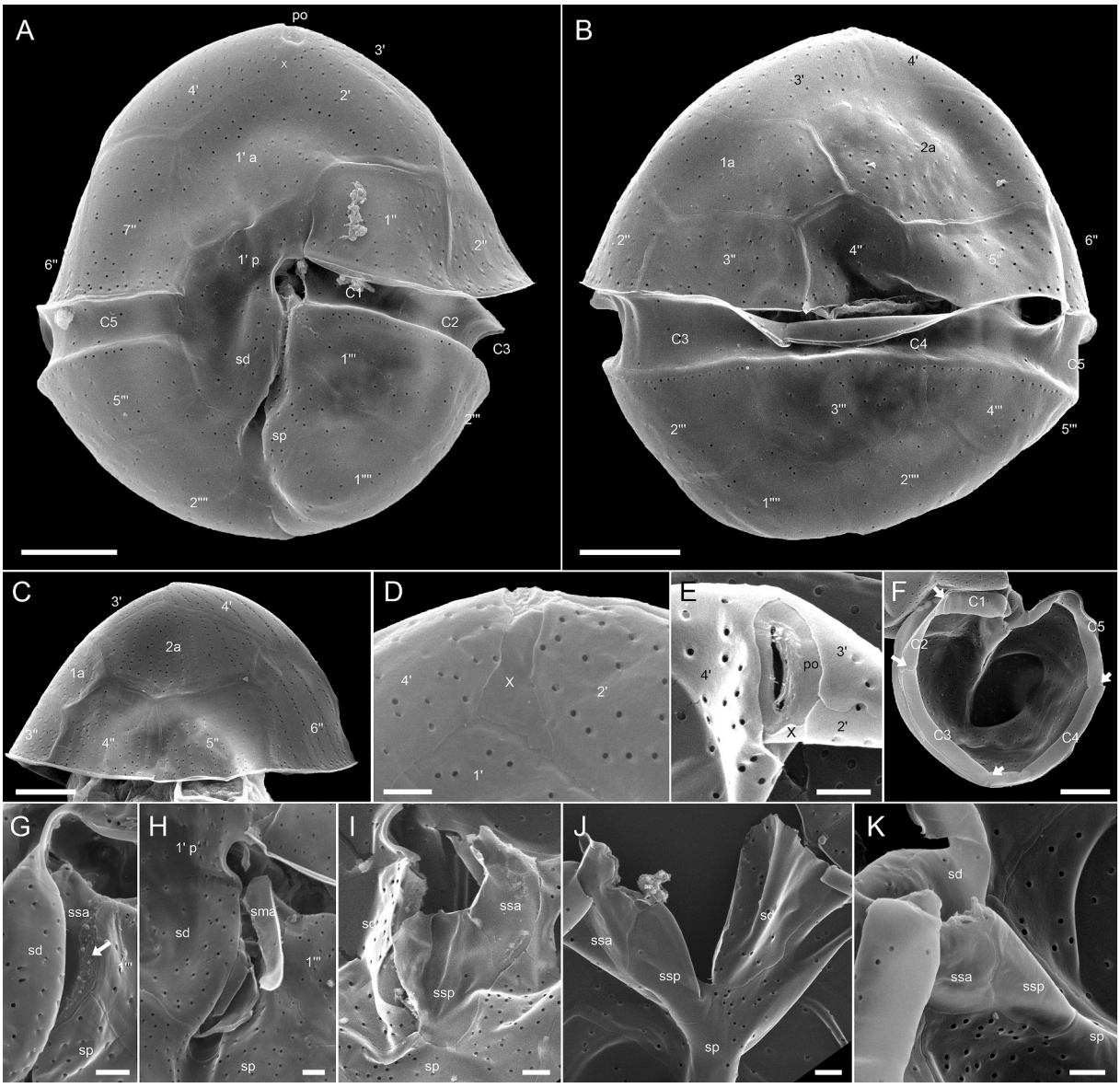

Fig. 4. *Kryptoperidinium secundum*, strain ARC121. Scanning electron microscopy of different thecae. (A) Cell in in ventral view. (B) Cell in dorsal view. (C) Epitheca in dorsal view. (D) Detailed view of the X-plate (canal plate). (E) Detailed view of the cell apex. (F) Apical view of the hypotheca showing cingular plates. (G–K) Detailed views of the central sulcal area. Plate labels according to the Kofoidean system, modified by labelling an anterior part (1′ a) and a posterior part (1′ p) of the first apical plate. Abbreviations: sd, right sulcal plate; sma, anterior median sulcal plate; sp, posterior sulcal plate; ssa, anterior left sulcal plate; ssp, posterior left sulcal plate. Scale bars: 5 μm (A–C, F), 1 μm (D, E, G–K).

was roughly rectangular and posteriorly abutted the right-anterior side of the large and asymmetric posterior sulcal plate (sp). The right and left anterior sides and the posterior part of plate sp were triangular, and the left anterior part had a broad contact to plate 1‴ (Fig. 3A–D, K–N, 4H). The small plates in the central sulcal area were difficult to retrieve by LM, but a tongue-shaped posterior left sulcal plate (ssp) was clearly visible, which abutted the anterior sulcal plate (sa) in a central notch. Another small and irregularly shaped plate constituted a right-hand extension of plate ssp (Fig. 3L–N, 4J, K). Moreover, a narrow, elongated plate (a median anterior sulcal plate: sma) was located on the left side of plate sd, and this plate often was brightly stained (Fig. 3L–N). The small and irregularly shaped plate sa abutted plates 1′ p and C1 and formed the anterior termination of the sulcus.

Thecal pore size was estimated 0.12–0.19 μm in diameter. A few plates were consistently free of pores including the pore plate and the X-plate (Fig. 4D). There was a row of pores on postcingular plates below the cingulum (Fig. 4A, B). Furthermore, SEM confirmed the existence of five cingular plates (Fig. 4E), but the arrangement of the small sulcal plates could not be determined further. Nevertheless, SEM confirmed that plates sd and 1‴ were tight in the central sulcal area and formed an inwardly bounded funnel (Fig. 4A). This funnel was composed by two inwardly bound, small plates, namely sma on the cell's right-lateral side and plate ssa on the cell's left-lateral side (Fig. 4G–K). Plate ssa had a partly rough surface (Fig. 4G), as if this plate and plate sma had been glued together. Plate sma had a characteristically spoon-like shape (Fig. 4H). In the central sulcal area, there was a larger and tongue-like plate ssp. (Fig. 4I–K). The small plate sa was probably lost or could not be clearly observed in SEM (Fig. 4G–H), although it was visible in LM (Fig. 3K–N).

3.3. Pigment profiles

Both strains revealed the same pigment profile with the chromatogram exemplarily shown for strain ARC121 in Fig. 6. The pigment

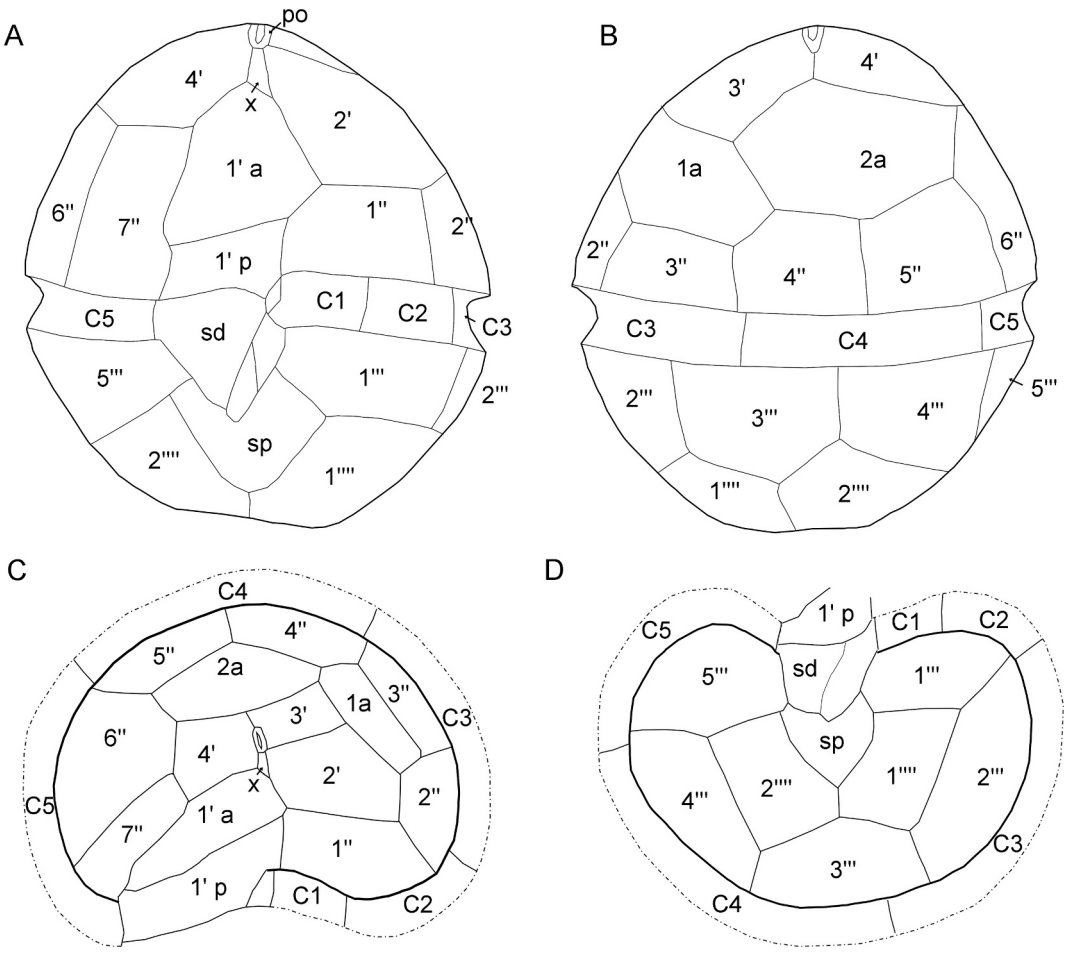

Fig. 5. Plate pattern (schematic line drawings) of *Kryptoperidinium secundum*. (A) Ventral view. (B) Dorsal view. (C) Epithecal plates in apical view. (D) Hypothecal plates in antapical view.

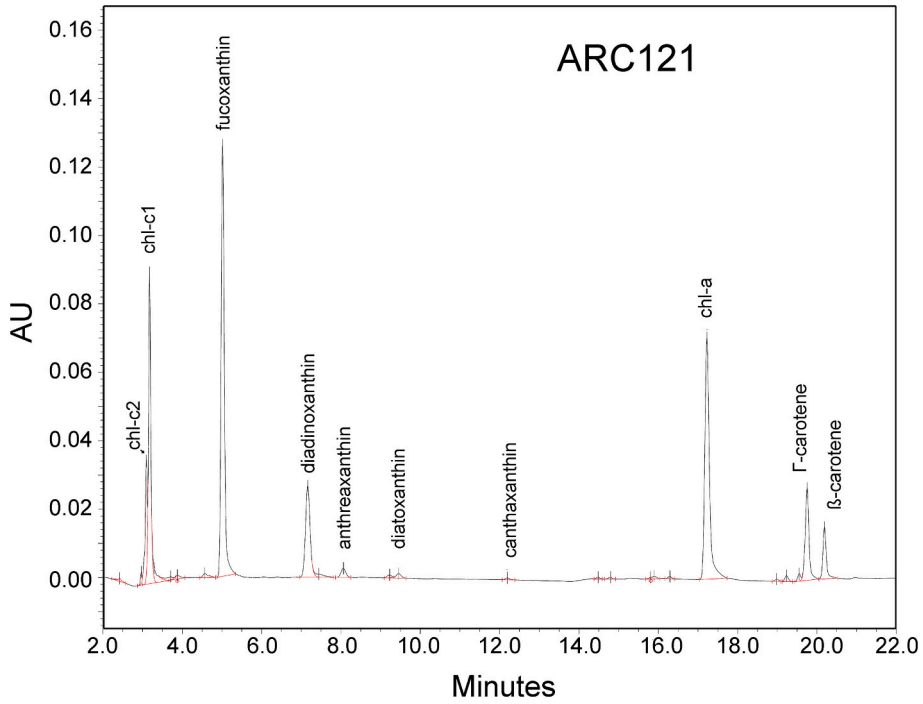

Fig. 6. HPLC chromatogram, pigment profile of *Kryptoperidinium secundum*, strain ARC121.

profile was dominated by chlorophylls *a*, *c1* and *c2* and by fucoxanthin as the major carotenoid. In addition, antheraxanthin, canthaxanthin, two carotenoids (ß and γ), diadinoxanthin and diatoxanthin were identified. To the contrary, the xanthophyll-cycle pigments violaxanthin and zeaxanthin were absent from strains ARC121 and ARC231, but present in some strains of *K. triquetrum* analysed in parallel (Table 2). There was no single pigment, which showed a consistent presence/absence between all strains of *K. triquetrum* and *K. secundum* (Table 2). The pigment cell quota in all strains were variable but for both strains ARC121 and ARC231, they were in the same order of magnitude as all other studied strains of *K. triquetrum* (Table 2).

3.4. Molecular phylogenetics

The SSU + ITS + LSU alignment of peridinialean dinophytes was 1822 + 786 + 2995 bp long and was composed of 458 + 553 + 740 parsimony-informative sites (31 %, mean of 21.89 per terminal taxon) and 2826 distinct RAxML alignment patterns. Figure 7 shows the best-scoring ML tree (−ln = 55,583.79), with many nodes showing high if not maximal support. The Kryptoperidiniaceae were monophyletic (98LBS, 1.00BPP) and were part of a clade (53LBS, 1.00BPP) including Blastodiniaceae (100LBS, 1.00BPP), Ensiculiferaceae (99LBS, 1.00BPP) and Zooxanthellaceae (single accession). Kryptoperidiniaceae comprised *Durinskia* (94LBS, 1.00BPP), *Blixaea* (single accession), *Unruhdinium* (100LBS, 1.00BPP), *Dinothrix* (100LBS, 1.00BPP) and *Kryptoperidinium*, whereas the latter two were closely related (100LB, 1.00BPP). *Kryptoperidinium* segregated into two clades, namely *K. triquetrum* (100LBS, 1.00BPP) and *K. secundum* (100LBS, 1.00BPP).

The SSU + ITS + LSU + *psb*A + *rbc*L + *psb*C alignment of diatoms was 1856 + 1134 + 3332 + 1005 + 1583 + 1414 bp long and was composed of 370 + 692 + 324 + 83 + 372 + 269 parsimony-informative sites (20 %, mean of 13.11 per terminal taxon) and 3973 distinct RAxML alignment patterns. Figure 8 shows the best-scoring ML tree (−ln = 55,538.33), with many nodes having high if not maximal statistical support. Dinophyte endosymbionts did not constitute a monophyletic group, with those of *Dinothrix*, *Durinskia* and *Kryptoperidinium* scattered over the tree in a polyphyletic pattern. Endosymbionts of *Kryptoperidinium* were retrieved as three only distantly related lineages (two of which associated with *K. triquetrum*) nested within the bacillariacean clade 6B (60LBS, 1.00BPP), which each had close relatives among free-living diatoms (all such relationships are highly supported). Endosymbionts of *K. secundum* were monophyletic (94LBS, 1.00BPP) and constituted the sistergroup (100LBS, 1.00BPP) of a clade harbouring (freshwater as well as marine) species of "*Nitzschia*" but also many undetermined bacillariacean diatoms from the field.

4. Discussion

4.1. Taxonomic delimitation of *Kryptoperidinium secundum sp. nov.*

The biodiversity assessment of dinophytes is far from complete. This does not only refer to rare species or those occurring in remote regions. For example, a new dinophyte was described from Germany recently, which was identified as the second most abundant species in the ponds of the Munich Botanical Garden in an annual monitoring programme (Müller et al., 2024). Similarly, the new species presented in this study belongs to an already long known, widely distributed and morphologically easily recognisable lineage of dinophytes, namely *Kryptoperidinium* (Ehrenberg, 1840; Lindemann, 1924). However, it is clearly distinct from *K. triquetrum* based on both morphological and molecular data and for the first time, we provide a comprehensive characterisation of *K. secundum*. The available data also indicate exclusive distributions of the two species, with *K. secundum* occurring in New World habitats (North Carolina, USA: this study; South Carolina, USA: Kempton et al., 2002; Maryland, USA: Wolny et al., 2022; and suspected in Florida, USA, and Virginia, USA: J. Wolny, unpublished data), while *K. triquetrum* is

Table 2
Pigments in the order of the retention times, in pg per cell for each strain. The number of total cells filtered is added as a biomass parameter. Abbreviations: n.d. = below detection limit.

strain	species	origin	cells per filter	chlorophyll *c2*	chlorophyll *c1*	fucoxanthin	violaxanthin	diadinoxanthin	antheraxanthin	diatoxanthin	zeaxanthin	canthaxanthin	chlorophyll *a*	gamma-carotene	beta-carotene
ARC121	*K. secundum*	USA	109,650	0.91	3.14	12.00	n.d.	2.18	0.18	0.14	n.d.	0.07	20.26	1.93	0.98
ARC231	*K. secundum*	USA	92,715	0.73	3.00	11.61	n.d.	1.83	0.10	0.13	n.d.	0.04	19.34	1.24	0.89
W4-A6	*K. triquetrum*	Wismar	32,410	1.56	6.35	24.09	0.09	5.71	0.12	0.22	n.d.	n.d.	41.54	1.87	2.20
W4-F9	*K. triquetrum*	Wismar	125,700	1.13	3.43	15.16	0.02	2.66	0.21	0.06	0.04	0.05	25.04	0.86	0.97
W1-D6	*K. triquetrum*	Wismar	46,700	2.73	8.66	37.30	0.06	5.48	0.43	0.14	0.05	0.09	63.44	1.49	2.46
W1-E4	*K. triquetrum*	Wismar	62,300	1.63	4.73	20.68	0.09	4.97	0.23	0.18	0.06	0.12	34.91	1.41	1.55
W1-D11	*K. triquetrum*	Wismar	165,800	1.79	5.62	24.14	0.06	3.53	0.35	0.09	0.02	0.14	42.17	1.22	1.73
G-E8	*K. triquetrum*	Greifswald	42,100	2.22	4.71	21.71	n.d.	3.31	0.26	0.08	n.d.	0.12	38.61	1.15	1.81
KFF 1001	*K. triquetrum*	Finland	20,400	1.77	4.87	17.56	n.d.	2.63	n.d.	n.d.	n.d.	n.d.	30.26	0.77	1.79
GeoB 459	*K. triquetrum*	Greece	29,750	0.93	3.10	12.60	n.d.	1.44	n.d.	n.d.	n.d.	n.d.	20.51	0.57	1.25

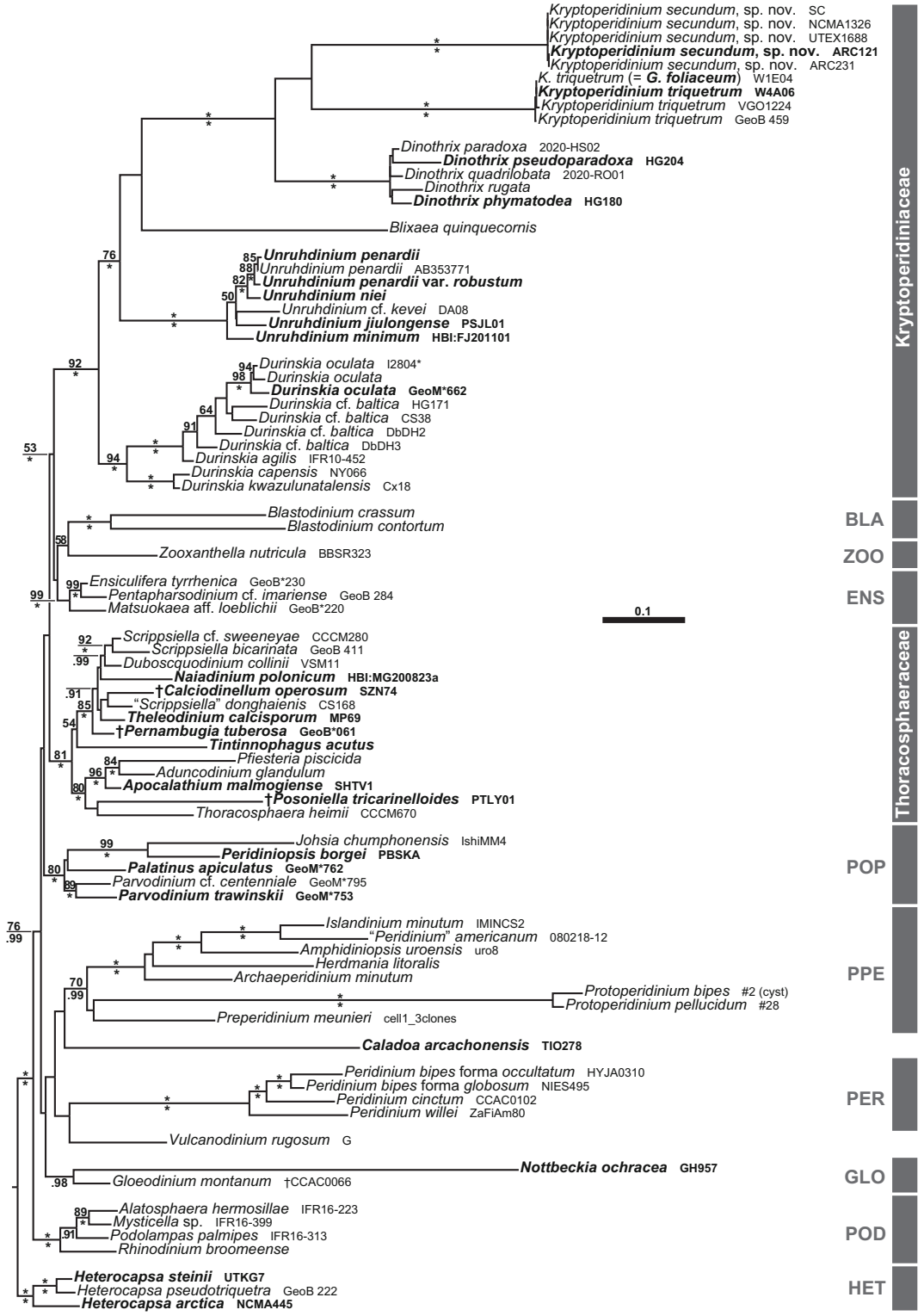

Fig. 7. A molecular reference phylogeny recognising major groups of Peridiniales. Maximum Likelihood (ML) tree of 80 systematically representative peridinialean sequences (−ln = 55,583.79) with a focus on Kryptoperidiniaceae (with strain number information) as inferred from a concatenated rRNA nucleotide alignment (1751 parsimony-informative positions). Numbers on branches are ML bootstrap (above) and Bayesian probabilities (below) for the clusters (asterisks indicate maximal support values, values under 50 and 0.90, respectively, are not shown). Equivalents of type (or at least reference) material is indicated by bold lettering. Abbreviations: BLA Blastodiniaceae; ENS, Ensiculiferaceae; HET, Heterocapsaceae; GLO, Gloeodiniaceae; PER, Peridiniaceae; POD, Podolampaceae; POP, Peridiniopsidaceae; PPE, Protoperidiniaceae; ZOO, Zooxanthellaceae.

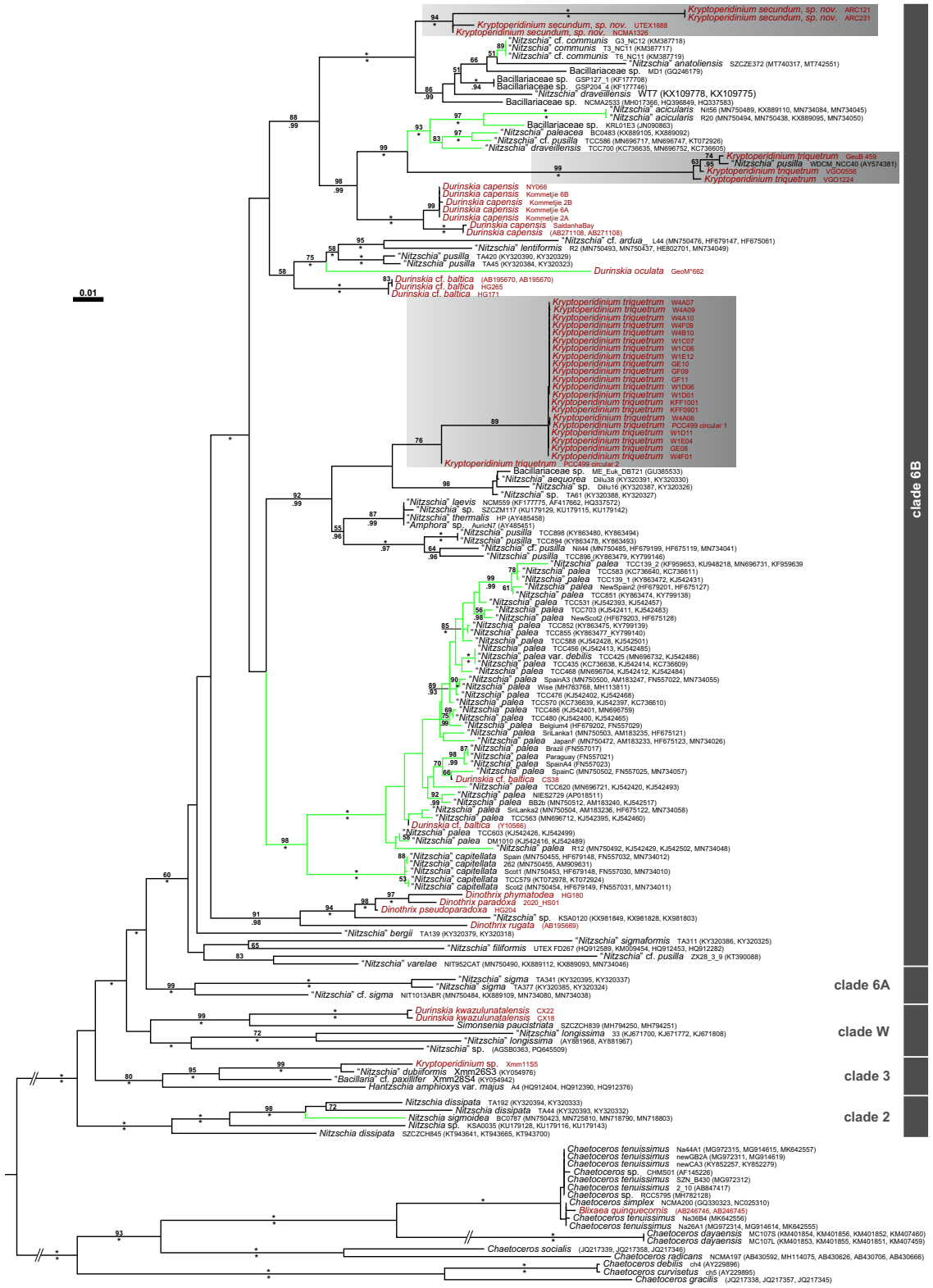

Fig. 8. A molecular reference tree recognising major groups of Bacillariaceae, with a focus on clade 6B harbouring many dinophytes' endosymbionts. Maximum Likelihood (ML) tree of 161 bacillariacean sequences (with strain number and GenBank accession number information and using *Chaetoceros* Ehrenberg as outgroup) as inferred from an alignment comprising concatenated sequences of the rRNA complex, *psb*A, *rbc*L and *psb*C (2110 parsimony-informative positions). Clade labelling follows previous work (Mann et al., 2021). Numbers on branches are ML bootstrap (above) and Bayesian probabilities (below) for the clusters (asterisks indicate maximal support values, values under 50 and 0.90, respectively, are not shown). Note that endosymbionts of Kryptoperidiniaceae (emphasised by red lettering) are scattered over the tree in a highly polyphyletic pattern, accessions assigned to *Kryptoperidinium* are shaded grey. Freshwater accessions are highlighted by green branches.

present in Europe (Tillmann et al., 2023).

The morphological delimitation of *K. secundum* from the type species *K. triquetrum* is based on a striking detail of the thecal plates. In *K. triquetrum*, the distalmost precingular plate is characteristically L-shaped and narrow and has a distinctly thin and elongated base, whereas it is mostly rectangular and relatively broad in *K. secundum*, only occasionally showing a modest indication of a slightly widened base (Fig. 9). The thecal plates, and especially the lateral precingular plates, are certainly difficult to observe and to distinguish in regular LM. However, the differential shapes of plate 7″ are very clear in the two species of *Kryptoperidinium* using fluorescence microscopy and plate staining. Under this condition, plate 7″ is clearly distinguishable from the adjacent plates by bright fluorescence in *K. triquetrum* only, but not in *K. secundum* (Fig. 9).

In several studies of European *Kryptoperidinium*, the diagnostic shape of plate 7″ has been neither mentioned nor illustrated nor even observed (Lindemann, 1924; Lebour, 1925). Instead, the first apical plate has been occasionally confused with a precingular plate and the narrow plate 7″ overlooked, leading to a plate formula comprising only six precingular plates (Lebour, 1925). Notably, van Goor (1925) was first who observed and drew plate 7″, although he (and later Biecheler, 1952) emphasised the challenge to detect this plate under LM. The suture between plates 1′ and 7″ appears "… barely visible …" (Germ. "… nur sehr schwerlich sichtbar …"; van Goor, 1925: 278) and out of many cells examined, only ten allow at least a partial confirmation of plate 7″. Biecheler (1952) concurred with van Goor (1925) and acknowledged the difficult observation of this plate. She concluded that its existence was probable but not certain, hence her notation of "6–7 precingular" plates in the formula of *Kryptoperidinium*. Such challenging allocation of the narrow plate 7″ might also explain why its basal elongation is depicted neither in van Goor (1925) nor in Biecheler (1952), despite of its presence in *K. triquetrum* (Satta et al., 2020; Tillmann et al., 2023).

Beyond the distalmost precingular plate, the distinction of both *K. triquetrum* (Tillmann et al., 2023) and *K. secundum* is not possible using regular LM, because of the high variability regarding cell size and shape. Furthermore, the two species consistently share a similar eyespot and the tertiary endosymbiosis with a diatom, illustrated by the second nucleus additionally to the dinophyte nucleus. The striking formation of brown globules in cells of *K. secundum* during stationary growth phase is unknown from *K. triquetrum*, which exhibits red inclusions (Tillmann et al., 2023). However, systematic studies are needed to enlighten whether this anecdotal report establishes a diagnostic trait between the two species. Whether one or both species of *Kryptoperidinium* generate harmful ecological effects as assumed earlier (Lindemann, 1924; Lewitus et al., 2003; Turki et al., 2007) remains another open research question.

4.2. Critical reception of supposedly deviating morphologies

Both species of *Kryptoperidinium* exhibit an identical thecal plate pattern, as demonstrated for *K. triquetrum* based on 23 strains (including

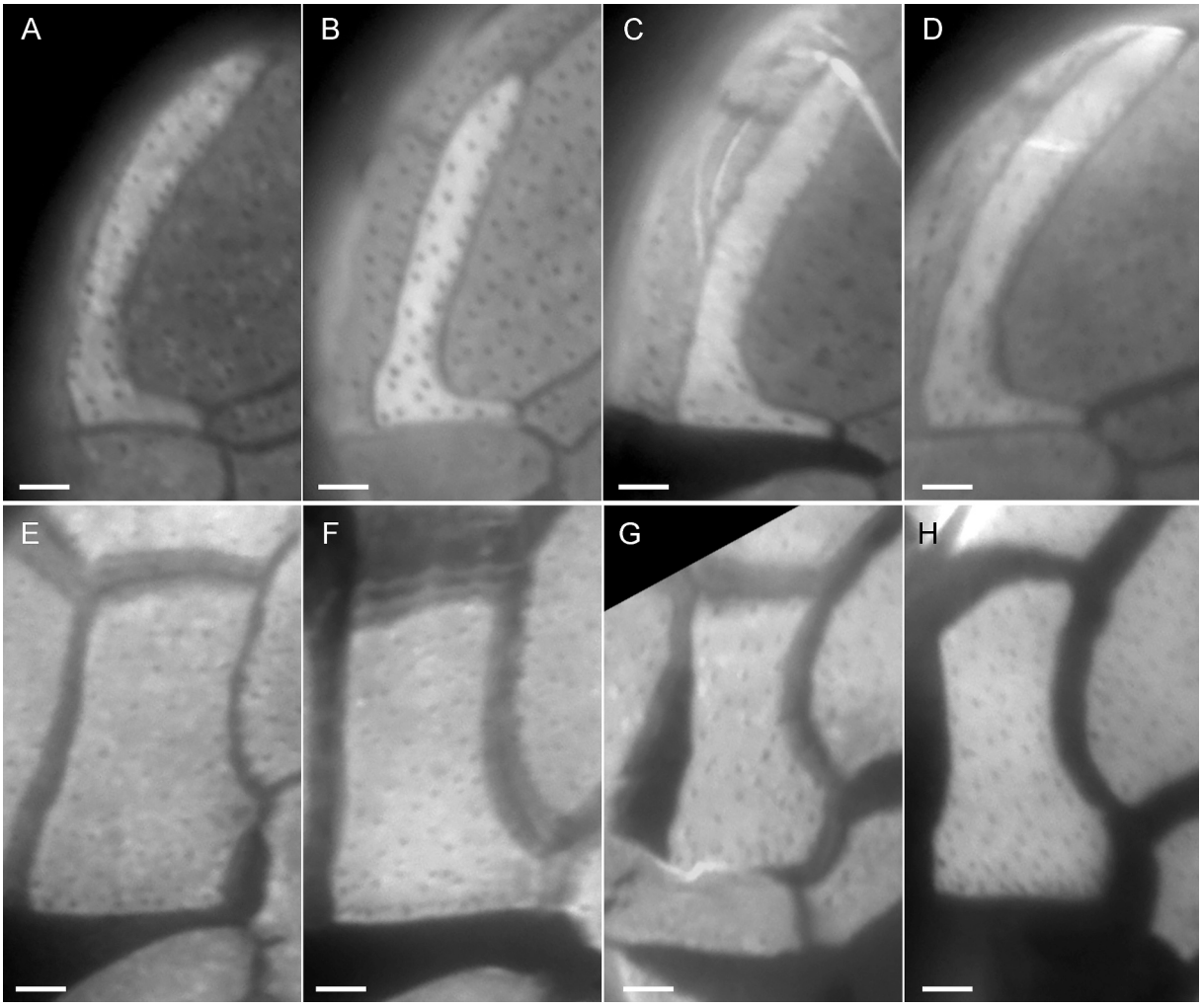

Fig. 9. Comparison of shape and appearance of the distalmost precingular plate 7″ in *Kryptoperidinium triquetrum* (A–D) and *Kryptoperidinium secundum* (E–H). (A, B) Strain W4-F9. (C) Strain GE-8. (D) Strain W1-E9 (for strain information see Tillmann et al., 2023). (E–G) Strain ARC121. (H) Strain ARC231. Scale bars = 2 µm.

the epitype strain) from different regions of the world (Tillmann et al., 2023) and here for at least two strains (including the type strain) of *K. secundum*. There might be more species of *Kryptoperidinium* (potentially with divergent plate patterns), but it seems very likely that at least some deviations already reported in the literature are rather erroneous observations or misinterpretations (see Table 2 in Tillmann et al., 2023). They include the questionable reports of six (instead of seven) precingular plates (Lindemann, 1924; Lebour, 1925), three (instead of four) apical plates (Figueroa et al., 2009) and six (instead of five) cingular plates (Trigueros et al., 2000). It is, again, worthy to note that the thecal plates are very delicate in *Kryptoperidinium* and therefore challenging to identify reliably.

The report of seemingly four cingular plates (Kempton et al., 2002; Figueroa et al., 2009) is of particular interest as both species of *Kryptoperidinium* have been already compared (though *K. secundum* then still unnamed). Four cingular plates are stated for all three studied strains of *K. secundum*, but Kempton et al. (2002) did not provide corresponding micrographs. It is doubtlessly difficult to clearly identify plate sutures in lateral views of *Kryptoperidinium*, and this refers particularly to the cell's left-lateral cingular area with the suture between plates C2 and C3. However, the present analysis has put attention to this trait and consistently shows five cingular plates in both strains of *K. secundum* under investigation (like in *K. triquetrum*) that differences in the numbers of cingular plates are unlikely between both species now known.

The cingular displacement has been additionally considered a diagnostic trait, supposedly being descending in *K. secundum* and ascending in *K. triquetrum* (Kempton et al., 2002). However, cells of *Kryptoperidinium* quickly lose their shape upon fixation or squeezing under a coverslip that subsequently, the original and natural position of the cingulum is difficult to evaluate. If this is considered, then careful observation of living cells confirms the cingulum being displaced neither in *K. triquetrum* nor in *K. secundum*, corroborating previous reports (van Goor, 1925; Biecheler, 1952).

Both strains under present investigation, and multiple strains of *K. triquetrum* from different areas (Tillmann et al., 2023), are bi-nuclear, but strain SC (now identified as *K. secundum*) may lack the diatom-derived nucleus (Kempton et al., 2002). This would be reminiscent of some other dinotoms such as *Durinskia yukatanensis* Okolodkov, Steidinger & Gárate-Lizárraga and *Unruhdinium niei* (G.X.Liu & Z.Y.Hu) Gottschling, having only one nucleus based on acetocarmine staining (Zhang et al., 2011; Okolodkov et al., 2024). Moreover, *D. capensis* Pienaar, H.Sakai & T.Horiguchi is kleptoplastidic, keeps the endosymbiont only temporarily for a maximum of a few months and therefore repeatedly needs to capture its associating diatom *Nitzschia captiva* D.G. Mann, Trobajo, Witkowski, Nor.Yamada & J.J.Bolton (Yamada et al., 2019; Mann et al., 2023). All these data may indicate that the endosymbiosis between the diatom and its dinophyte host is not always obligate (Žerdoner Čalasan et al., 2018; Tillmann et al., 2023), but it is worth noting that the nuclear variation appears at the species level and not at the strain level in dinotoms. In *Kryptoperidinium*, it is strain SC only that may lack the diatom nucleus implying a more transient endosymbiosis (Kempton et al., 2002) although, the other two strains of *K. secundum* studied here in fact exhibit the second nucleus. Intraspecific variability appears unlikely in such an important trait as a photosynthetically active partner, and it is difficult to demonstrate the absence of a structure unambiguously. Furthermore, the diatom nucleus often stains only faintly compared to the bright and large dinophyte nucleus and might thus be masked by the other nucleus and/or plastids. It is, thus, not impossible that a second nucleus has remained undetected occasionally (Kempton et al., 2002; Gottschling et al., 2019).

Pigment profiles have been considered to delimitate the two species of *Kryptoperidinium*. Based on a previous study (Kempton et al., 2002), three strains, whose sequence data now identify them as *K. secundum* (i.e., NCMA1326, SC, UTEX1688), show identical pigment compositions, whereas the two strains of *K. triquetrum* (i.e., CCAP1116/3 and CS291) differ from the others due to the presence of canthaxanthin and zeaxanthin. The absence of zeaxanthin is discovered in both strains of *K. secundum* studied here, although antheraxanthin, which is the intermediate of zeaxanthin and violaxanthin in the xanthophyll cycle, is detected. Half of the strains determined as *K. triquetrum* show no detectable traces of this pigment. Likewise in contrast to Kempton et al. (2002), both strains of *K. secundum* contain canthaxanthin, whereas this pigment is absent in, again, approximately half of the strains assigned to *K. triquetrum*. Thus, diagnostic pigment profiles between the two species of *Kryptoperidinium* are not supported by the present analysis.

4.3. Life history

Dinophytes exhibit complex developmental processes, and morphologically similar cell types can be involved in completely different processes of vegetative replication or sexual reproduction (Pfiester and Anderson, 1987; Figueroa et al., 2018). For example, planospores hatched from a sporocyst may serve asexual replication but be morphologically indistinguishable from gametes that will fuse to form a zygote. The regular mitotic division in *K. secundum* occurs by eleutheroschisis, which is prevalent among the Peridiniales (Kwok et al., 2023). Only the early lineages of this group (Gottschling et al., 2024), namely Heterocapsaceae (Tillmann et al., 2017) and Podolampaceae (Mertens et al., 2023), divide by the fundamentally different process of desmoschisis (which might be ancestral in the Peridiniales by outgroup comparison).

Eleutheroschisis can occur in different ways within the Peridiniales. In the Peridiniaceae, the two daughter cells develop within the parental theca (Lefévre, 1932; Pfiester and Anderson, 1987; Gürkan et al., 2024), which thus becomes a sporocyst. At maturity, the parental theca opens (usually along sutures separating the thecal plates) and the planospores escape, which are usually only provided with a weakly developed new theca. In contrast, Kryptoperidiniaceae appear different and virtually unique within the Peridiniales in that the (usually two, occasionally four or eight) daughter cells are formed in a delicate sheath, the pellicle (Penard, 1891; Kretschmann et al., 2018; Tillmann et al., 2023). The pellicle shows no signs of a parental theca, and it is still unclear how such a sporocyst is formed. The sporocysts of the Kryptoperidiniaceae are morphologically similar to those of the phytodinialean Borghiellaceae (Lindemann, 1929; Daugbjerg et al., 2014; Müller et al., 2024) and Tovelliales (Pandeirada et al., 2017), although they are only distantly related to these subordinate groups of dinophytes (Gottschling et al., 2024). Whether the absence of dormant stages in *K. secundum* distinguishes the species from *K. triquetrum* exhibiting such cells (Tillmann et al., 2023) remains another question for future research.

Sexual processes are also unknown or poorly understood in many dinophytes (Bhaud et al., 1988; Pfiester, 1989; Figueroa et al., 2018). The small, fast and eventually mating swarmers observed in *K. secundum* may function as gametes. However, it remains elusive how thecate cells can fuse together – in *Peridinium* Ehrenberg, the planozygote arises after shedding the gamete thecae and exhibits a newly formed shell with the same pattern as that of the vegetative cells (Pfiester, 1976). Such a process could not be observed in *K. secundum*. Knowledge of the ploidy levels of individual cells would considerably advance the understanding of sexual processes in dinophytes – methodologically, however, such investigations remain a great challenge.

4.4. Plastid capture

In times gone by, the Kryptoperidiniaceae have not been recognised as distinct from other dinophytes that host a peridinin plastid. However, ultrastructural analyses have shown that Kryptoperidiniaceae have an endosymbiont that has itself already incorporated a eukaryotic alga (Dodge, 1971; Tomas et al., 1973), so that a tertiary level of integration is achieved. The result is organisms that comprise five genomes: those of two eukaryotic nuclei (which were also demonstrated in this study), two

origins of mitochondria, and the plastid of diatom-origin. Tertiary endosymbioses are very well known from dinophytes, and they have arisen several times independently within the group (e.g., in Brachydiniaceae: Yoon et al., 2005; Dorell and Howe, 2015; and Dinophysaceae: Schnepf and Elbrächter, 1988; Garcia-Cuetos et al., 2010). The remarkable diversity of heterotrophy in dinophytes is sometimes considered an ecological licence for these parallel evolutionary origins (Schnepf and Elbrächter, 1999).

Comparably, it was previously assumed that Kryptoperidiniaceae inherit their endosymbionts vertically (Tippit and Pickett-Heaps, 1976), which may be correct for some species of dinotoms. However, if vertical heredity also takes place in geological scale and thus a co-divergence would prevail, then phylogenetic trees built by the dinophyte hosts and their endosymbionts would have to be congruent. However, research in recent years has repeatedly questioned this hypothesis, as the corresponding phylogenetic trees have only limited congruence (Žerdoner Čalasan et al., 2018; Tillmann et al., 2023). Instead, the endosymbionts of the Kryptoperidiniaceae usually appear to be species-specific, but they often have close relatives among free-living diatoms, as is also shown here for *K. secundum*. From these findings, an evolutionary scenario can be constructed, in which Kryptoperidiniaceae have acquired the endosymbionts both horizontally and vertically: by the repeated uptake of different free-living diatoms (Žerdoner Čalasan et al., 2018; Tillmann et al., 2023) and maintain them by inheriting the absorbed endosymbionts through synchronous cell division (Figueroa et al., 2009).

4.5. Character evolution of thecal plate pattern

The evolutionary history of dinophytes and the origin of their thecal plate pattern has long attracted scientific interest. The plate arrangement of the hypotheca appears very conserved, and most Peridiniales (including Kryptoperidiniaceae) share five postcingular and two antapical plates (or less). As inferred from an integrative approach combining molecular and morphological data (Tillmann et al., 2021), the five derive from six postcingular plates (today abundant in dinophytes outside the Peridiniales), and this trait is an apomorphy of the Peridiniales from an evolutionary perspective (Gottschling et al., 2021).

The number of epithecal plates is more variable and as a rule, fewer rather than more epithecal plates may represent phylogenetically derived states in peridinialean dinophytes. Particularly, the number of intercalary plates varies, drastically exemplified by the Peridiniopsidaceae encountering three, two, one or no such plates (Kretschmann et al., 2019). Kryptoperidiniaceae appear rather homogeneous in this respect always exhibiting two intercalary plates that may derive from three such plates predominantly present in the Peridiniales. However, two intercalary plates are also found in (most) Peridiniopsidaceae, (some) Protoperidiniaceae and (few) Thoracosphaeraceae, and such reductions must be considered independent evolutionary events as inferred from the only distant relationships of the corresponding lineages.

Seven precingular plates are abundant in peridinialean dinophytes and may indicate the ancestral state, whereas six precingular plates are mostly found in smaller and monophyletic species groups such as diplopsalean and pfiesterian dinophytes (Calado et al., 2009), indicating the derived character state. However, the number of precingular plates is puzzling within Kryptoperidiniaceae: The members with seven precingular plates (i.e., *Blixaea*, *Dinothrix*, *Kryptoperidinium*) appear to constitute a monophyletic group, whereas those with predominantly six precingular plates (i.e., *Durinskia*, *Unruhdinium*) comprise a paraphyletic grade. Either, the last common ancestor of Kryptoperidiniaceae had six precingular plates, which reverted once back to seven such plates in *Blixaea*, *Dinothrix* and *Kryptoperidinium* (for which there is no evidence); or, the seven precingular plates of the latter species group in fact represent the ancestral state, and a reduction to six such plates evolved twice independently in *Durinskia* and *Unruhdinium* – both interpretations are likewise parsimonious.

Most species of *Durinskia* have six precingular plates, but *Durinskia agilis* (Kofoid & Swezy) Saburova, Chomérat & Hoppenrath is a notable exception: The benthic species described from intertidal sand flats of Kuwait (Saburova et al., 2012a) exhibits the same plate pattern as *Kryptoperidinium* (i.e., 4′, 2a, 7″, 5C, 5‴, 2⁗). *Durinskia agilis* and *K. secundum* are also similar in size and shape, and both are dorsoventrally compressed, possess a distinct eyespot and can contain red and/or brown globules in the cytoplasm. However, they differ by an apparent apical hook at the epithecal pole only present in *D. agilis*, which is a projection of the fourth apical plate. Additionally, plate 7″ of *D. agilis* is wider than long whereas in *Kryptoperidinium*, this plate is longer than wide. Most strikingly, the first apical plate of *Kryptoperidinium* is divided into two parts by an oblique suture (Tillmann et al., 2023), now also confirmed for *K. secundum*. This trait is not found in any other dinotom (including *Dinothrix* and *D. agilis*) or even the entirety of Peridiniales, making it a remarkable synapomorphy and diagnostic trait of the two species now assigned to *Kryptoperidinium*, namely *K. triquetrum* and *K. secundum*. Although the statistical support for entire *Kryptoperidinium* is not overwhelming in molecular phylogenetics (Fig. 7), the shared synapomorphy of a divided first apical plate, and only minor morphological differences between *K. triquetrum* and *K. secundum*, do not justify their separation at generic rank.

5. Formal taxonomy

Kryptoperidinium secundum Tillmann, Wolny & Gottschling sp. nov.—Type [illustration]: USA–NC. Brown Creek, Neuse River: [A.O. Tatters ARC121] s.n. (holotype, designated here: Fig. 1 G–J!) [http://phycobank.org/105773].

Description: Dinophytes phototrophic, hosting a diatom endosymbiont, thecate. Flagellated cells 18–37 µm in diameter, dorso-ventrally compressed, in ventral view with asymmetrically round episome and more symmetric and round hyposome; cingulum median, discontinuous in the central ventral area; thecal plates thin, delicate; thecal pores numerous, small, arranged in rows on some dorsal plates; tabulation po, X, 4′, 2a, 7″, 5C, 6(?)s, 5‴, 2⁗; first apical plate subdivided into a posterior and anterior part; distalmost precingular plate rectangular, half as wide as long. Compartments distinct; plastids numerous, small, globular to ellipsoid or slightly elongated; dinophyte nucleus large, in the left side of the cell centre; diatom nucleus small, irregularly shaped. Division stages present; two (or occasionally four or eight) cells included in the pellicle during deflagellated stage.

Habitat: Marine/brackish water column.

Etymology: The epithet *secundum* (lat: secundus, the second) reflect that this is the second species of *Kryptoperidinium*.

Note: A detailed description of the strain, from which the type material was prepared, is provided in the Results section and a diagnosis in the Discussion section.

CRediT authorship contribution statement

Urban Tillmann: Writing – review & editing, Writing – original draft, Validation, Formal analysis, Conceptualization. **Marc Gottschling:** Writing – review & editing, Writing – original draft, Visualization, Formal analysis, Conceptualization. **Stephan Wietkamp:** Writing – review & editing, Formal analysis. **Ilka Peeken:** Writing – review & editing, Formal analysis. **Jennifer Wolny:** Writing – review & editing, Formal analysis. **Norico Yamada:** Writing – review & editing, Formal analysis.

Funding sources

This work was funded by the PACES II research program of the Alfred-Wegener-Institute (AWI) as part of the Helmholtz Foundation initiative in Earth and Environment.

Declaration of competing interest

The authors declare that they have no known competing financial interests or personal relationships that could have appeared to influence the work reported in this paper.

Acknowledgements

The authors would like to thank Anne Müller (Bremerhaven) for her technical assistance with algal culturing and Rafael Matysiuk (Munich) for providing the computational power for the phylogenetic analyses. The authors acknowledge support by the Open Access Publication Funds of AWI.

Appendix A. Supplementary data

Supplementary data to this article can be found online at https://doi.org/10.1016/j.protis.2025.126120.

Data availability

Data will be made available on request.

References

Alkawri, A., 2016. Seasonal variation in composition and abundance of harmful dinoflagellates in Yemeni waters, southern Red Sea. Mar. Poll. Bull. 112, 225–234.

Baharudin, S.N., Hii, K.S., Azmi, N.F.M., Kassim, N.S., Abdullah, N., Teng, S.T., Liu, M., Kuwata, K., Iwataki, M., Gu, H., Lim, P.T., Leaw, C.P., 2025. High molecular diversity of potentially harmful heterotrophic dinophytes in tropical shrimp aquaculture ponds reveals a new dinophyte *Malayana penaeicida* gen. et sp. nov. (Peridiniales, Dinophyceae). Harmful Algae, 102906.

Barlow, R.G., Cummings, D.G., Gibb, S.W., 1997. Improved resolution of mono- and divinyl chlorophylls a and b and zeaxanthin and lutein in phytoplankton extracts using reverse phase C-8 HPLC. Mar. Ecol. Prog. Ser. 161, 303–307.

Bhaud, Y., Soyer-Gobillard, M.O., Salmon, J.M., 1988. Transmission of gametic nuclei through a fertilization tube during mating in a primitive dinoflagelate. *Prorocentrum micans*. Ehr. J. Cell Sci. 89, 197–206.

Biecheler, B., 1952. Recherches sur les Péridiniens. Bull. Biol. Fr. Belg. Supplement 36, 1–149.

Bricheux, G., Mahoney, D.G., Gibbs, S.P., 1992. Development of the pelliele and thecal plates following ecdysis in the dinoflagellate *Glenodinium foliaceum*. Protoplasma 168, 159–171.

Calado, A.J., Craveiro, S.C., Daugbjerg, N., Moestrup, Ø., 2009. Description of *Tyrannodinium* gen. nov., a freshwater dinoflagellate closely related to the marine *Pfiesteria*-like species. J. Phycol. 45, 1195–1205.

Chacón, J., Gottschling, M., 2020. Dawn of the dinophytes: a first attempt to date origin and diversification of harmful algae. Harmful Algae 97, 101871.

Daugbjerg, N., Andreasen, T., Happel, E., Pandeirada, M.S., Hansen, G., Craveiro, S.C.F., A.J., C., Moestrup, Ø., 2014. Studies on woloszynskioid dinoflagellates VII. Description of *Borghiella andersenii* sp. nov.: Light and electron microscopy and phylogeny based on LSU rDNA. Eur. J. Phycol. 49, 436–449.

Dodge, J.D., 1971. A dinoflagellate with both a mesocaryotic and a eucaryotic nucleus I. Fine structure of the nuclei. Protoplasma 73, 145–157.

Dodge, J.D., Crawford, D.W., 1969. Observations on the fine structure of the eyespot and associated organelles in the dinoflagellate *Glenodinium foliaceum*. J. Cell Sci. 5, 479–493.

Domingues, R.B., Anselmo, T.P., Barbosa, A.B., Sommer, U., Galvão, H.M., 2011. Nutrient limitation of phytoplankton growth in the freshwater tidal zone of a turbid. Mediterranean estuary. Estuar. Coast. Shelf Sci. 91, 282–297.

Dorell, R.G., Howe, C.J., 2015. Integration of plastids with their hosts: Lessons learned from dinoflagellates. Proc. Natl. Acad. Sci. U. S. A. 112, 10247–10254.

Droop, M.R., 1958. Requirements for thiamine among some marine and supro-littoral protista. J. Mar. Biol. Ass. U.K 37, 323–329.

Ehrenberg, C.G., 1840. [274 Blätter von ihm selbst ausgeführterZeichnungen von eben so vielen Arten]. Ber. Bekanntm. Verh.Königl. Preuss. Akad. Wiss. Berlin 1840, 197–219.

Figueroa, R.I., Bravo, I., Fraga, S., Garcés, E., Llaveria, G., 2009. The life history and cell cycle of *Kryptoperidinium foliaceum*, a dinoflagellate with two eukaryotic nuclei. Protist 160, 285–300.

Figueroa, R.I., Estrada, M., Garces, E., 2018. Life histories of microalgal species causing harmful blooms: Haploids, diploids and the relevance of benthic stages. Harmful Algae 73, 44–57.

Garcia-Cuetos, L., Moestrup, Ø., Hansen, P.J., Daugbjerg, N., 2010. The toxic dinoflagellate *Dinophysis acuminata* harbors permanent chloroplasts of cryptomonad origin, not kleptochloroplasts. Harmful Algae 9, 25–38.

van Goor, A.C.J., 1925. Einige Bemerkenswerte Peridineen des holländischen Brackwassers. Rec. Trav. Bot. Néerl. 22, 275–291.

Gottschling, M., 2017. Two new generic names for dinophytes harbouring a diatom as an endosymbiont, *Blixea* and *Unruhdinium* (Kryptoperidiniaceae, Peridiniales). Phytotaxa 306, 296–300.

Gottschling, M., Tillmann, U., Kusber, W.-H., Hoppenrath, M., Elbrächter, M., 2018. A Gordian knot: Nomenclature and taxonomy of *Heterocapsa triquetra* (Peridiniales: Heterocapsaceae). Taxon 67, 179–185.

Gottschling, M., Tillmann, U., Elbrächter, M., Kusber, W.-H., Hoppenrath, M., 2019. *Glenodinium triquetrum* Ehrenb. Is a not species of *Heterocapsa* F.Stein but of *Kryptoperidinium* Er.Lindem. (Kryptoperidiniaceae, Peridiniales). Phytotaxa 391, 155–158.

Gottschling, M., Carbonell-Moore, M.C., Mertens, K.N., Kirsch, M., Elbrächter, M., Tillmann, U., 2021. *Fensomea setacea*, gen. & sp. nov. (Cladopyxidaceae, Dinophyceae), is neither gonyaulacoid nor peridinioid as inferred from morphological and molecular data. Sci. Rep. 11, 12824.

Gottschling, M., Wietkamp, S., Bantle, A., Tillmann, U., 2024. Oxytoxaceae are prorocentralean rather than peridinialean dinophytes and taxonomic clarification of heterotrophic *Oxytoxum lohmannii* (≡ "*Amphidinium*" *crassum*) by epitypification. Sci. Rep. 14, 6689.

Grøntved, J., 1950. The phytoplankton of the Præstø Fjord. Folia Geogr. Dan. 3, 1–96.

Gürkan, S., Stemplinger, B.A., Rockinger, A., Knechtel, J., Gottschling, M., 2024. Bumps on the back: an unusual morphology in phylogenetically distinct *Peridinium* aff. *cinctum* (= *Peridinium tuberosum*; Peridiniales, Dinophyceae). Org. Divers. Evol. 24, 1–15.

Hallegraeff, G.M., Bolch, C.J.S., Hill, D.R.A., Jameson, I., LeRoi, J.M., McMinn, A., Murray, S., de Salas, M.F., Saunders, K., 2010. Algae of Australia - Phytoplankton of Temperate Coastal Waters. CSIRO, Melbourne.

Horiguchi, T., 2004. Origin and evolution of dinoflagellates with a diatom endosymbiont. In: Mawatari, S.F., Okada, H. (Eds.), Proceedings of the International Symposium on 'Dawn of a New Natural History—Integration of Geoscience and Biodiversity Studies'. Hokkaido University, Sapporo, pp. 53–59.

Katoh, K., Standley, D.M., 2013. MAFFT Multiple Sequence Alignment Software Version 7: Improvements in Performance and Usability. Mol. Biol. Evol. 30, 772–780.

Keller, M.D., Selvin, R.C., Claus, W., Guillard, R.R.L., 1987. Media for the culture of oceanic ultraphytoplankton. J. Phycol. 23, 633–638.

Kempton, J.W., Wolny, J., Tengs, T., Rizzo, P., Morris, R., Tunnell, J., Scott, P., Steidinger, K., Hymel, S.N., Lewitus, A.J., 2002. *Kryptoperidinium foliaceum* blooms in South Carolina: a multi-analytical approach to identification. Harmful Algae 1, 383–392.

Krakhmalny, A.F., Okolodkov, J.B., Bryantseva, Y.V., Sergeeva, A.V., Velikova, V.N., Derezyuk, N.V., Terenko, G.V., Kostenko, A.G., Krakhmalny, M.A., 2018. Revision of the dinoflagellate species composition of the Black Sea. Algologia 28, 428–448.

Kretschmann, J., Žerdoner Čalasan, A., Gottschling, M., 2018. Molecular phylogenetics of dinophytes harboring diatoms as endosymbionts (Kryptoperidiniaceae, Peridiniales), with evolutionary interpretations and a focus on the identity of *Durinskia aculata* from Prague. Mol. Phylogenet. Evol. 118, 392–402.

Kretschmann, J., Žerdoner Čalasan, A., Meyer, B., Gottschling, M., 2019. Zero intercalary plates in *Parvodinium* (Peridiniopsidaceae, Peridiniales) and phylogenetics of *P. elpatiewskyi,* comb. nov. Protist 171, 1–13.

Kwok, A.C.M., Chan, W.S., Wong, J.T.Y., 2023. Cell wall deposition with ecdysis and cellular growth. Mar. Drugs 21, 70.

Lebour, M.V., 1925. The Dinoflagellates of the Northern Seas. Marine Biological Association of the United Kingdom, Plymouth.

Lefévre, M., 1932. Monographie des espèces du genre *Peridinium*. Archives de Botanique. 2, 1–210.

Lewis, J., Taylor, J.D., Neale, K., Leroy, A.G., 2018. Expanding known dinoflagellate distributions: investigations of slurry cultures from Caspian Sea sediments. Bot. Mar. 61, 21–31.

Lewitus, A.J., Schmidt, L.B., Mason, L.J., Kempton, J.W., Wilde, S.B., Wolny, J.L., Williams, B.J., Hayes, K.C., Hymel, S.N., Keppler, C.J., Ringwood, A.H., 2003. Harmful algal blooms in South Carolina residential and golf course ponds. Popul. Environ. 24, 387–413.

Lindemann, E., 1924. Der Bau der Hülle bei *Heterocapsa* und *Kryptoperidinium foliaceum* (Stein) n. nom. (Zugleich eine vorläufige Mitteilung). Bot. Arch. 5, 114–120.

Lindemann, E., 1929. Experimentelle Studien über die Fortpflanzungserscheinungen der Süßwasserperidineen auf Grund von Reinkulturen. Arch. Protistenkd. 68, 1–104.

Mann, D.G., Trobaj, R., Sato, S., Li, C., Witkowski, A., Rimet, F., Ashworth, M.P., Hollands, R.M., Theriot, E.C., 2021. Ripe for reassessment: a synthesis of available molecular data for the speciose diatom family Bacillariaceae. Mol. Phylogenet. Evol. 158, 106985.

Mann, D.G., Yamada, N., Bolton, J.J, Witkowski, A., Trobajo, R., 2023. *Nitzschia captiva* sp. nov., the essential prey diatom of the kleptoplastic dinoflagellate *Durinskia capensis*, compared with *N. agnita, N. kuetzingioides* and other species, Phycologia 62, 136–151.

Mertens, K.N., Carbonell-Moore, M.C., Chomerat, N., Bilien, G., Boulben, S., Guillou, L., Romac, S., Probert, I., Ishikawa, A., Nezan, E., 2023. Morpho-molecular analysis of podolampadacean dinoflagellates (Dinophyceae), with the description of two new genera. Phycologia 62, 117–135.

Moestrup, Ø., Calado, A., 2018. Dinophyceae. Springer, Heidelberg.

Moldrup, M., Garm, A., 2012. Spectral sensitivity of phototaxis in the dinoflagellate *Kryptoperidinium foliaceum* and their reaction to physical encounters. J. Exp. Biol. 215, 2342–2346.

Müller, A., Stark, M., Schottenhammel, S., John, U., Chacon, J., Klingel, A., Holzer, V.J. C., Schöffer, M., Gottschling, M., 2024. The second most abundant dinophyte in the ponds of a Botanical Garden is a species new to science. J. Eukaryot. Microbiol. 71, e13015.

Okolodkov, Y.B., Cervantes-Urieta, V.A., Aguilar-Trujillo, A.C., Merino-Virgilio, F.C., Giuliana Cruz-Trejo, G., Huerta-Quintanilla, D.A., Steidinger, K.A., Gárate-Lizárraga, I.G., Durán-Riveroll, L.M., Herrera-Silveira, J.A., 2024. *Durinskia yucatanensis* sp. nov. (Peridiniales: Kryptoperidiniaceae), a new planktonic dinoflagellate species, and its habitat in coastal Yucatan waters, Gulf of Mexico. Hidrobiológica 34, 1–12.

Pandeirada, M.S., Craveiro, S.C., Daugbjerg, N., Moestrup, O., Calado, A., 2017. Studies on woloszynskioid dinoflagellates VIII: life cycle, resting cysts morphology and phylogeny of *Tovellia rinoi* sp. nov (Dinophyceae). Phycologia 56, 533–548.

Paulsen, O., 1908. XVIII. Peridiniales. In Brandt, K., Apstein, C., (eds) Nordisches Plankton. Lipsius & Tischer, Kiel, pp. 1–124.

Penard, E., 1891. Les Péridinacées du Léman. Bull. Soc. Bot. Genève 6, 1–63.

Pfiester, L.A., 1976. Sexual reproduction of *Peridinium willei* (Dinophyceae). J. Phycol. 12, 234–238.

Pfiester, L.A., 1989. Dinoflagellate sexuality. Int. Rev. Cytol. 114, 249–272.

Pfiester, L.A., Anderson, D.M., 1987. Dinoflagellate reproduction. In: Taylor, F.J.R. (Ed.), The Biology of Dinoflagellates. Academic Press, New York, pp. 611–648.

Prager, J.C., 1963. Fusion of the family Glenodiniaceae into the Peridiniaceae, with notes on *Glenodinium foliaceum* Stein. J. Protozool. 10, 195–204.

Pybus, C., McEvoy, S., McGrath, D., 1984. Red water caused by *Glenodinium foliaceum* (Dinophyta) in Lough Atalia, Co Galway. Ir. Nat. J. 21, 226–228.

Ronquist, F., Teslenko, M., van der Mark, P., Ayres, D.L., Darling, A., Höhna, S., Larget, B., Liu, L., Suchard, M.A., Huelsenbeck, J.P., 2012. MrBayes 3.2: Efficient Bayesian phylogenetic inference and model choice across a large model space. Syst. Biol. 61, 539–542.

Saburova, M., Chomerat, N., Hoppenrath, M., 2012a. Morphology and SSU rDNA phylogeny of *Durinskia agilis* (Kofoid & Swezy) comb. nov. (Peridiniales, Dinophyceae), a thecate, marine, sand-dwelling dinoflagellate formerly classified within *Gymnodinium*. Phycologia 51, 287–302.

Saburova, M., Polikarpov, I., Al-Yamani, F., 2012b. First record of *Kryptoperidinium foliaceum* (Dinophyceae: Peridiniales) from a hypersaline environment in Kuwait, north-western Arabian Gulf. Mar. Biodivers. Rec. 5, 1–7.

Satta, C.T., Pulina, S., Rene, A., Padedda, B.M., Caddeo, T., Fois, N., Luglie, A., 2020. Ecological, morphological and molecular characterization of *Kryptoperidinium* sp. (Dinophyceae) from two Mediterranean coastal shallow lagoons. Harmful Algae 97, 101855.

Schnepf, E., Elbrächter, M., 1988. Cryptophycean-like double membrane-bound chloroplast in the dinoflagellate, *Dinophysis* Ehrenb.: Evolutionary, phylogenetic and toxicological implications. Bot. Acta 101, 196–203.

Schnepf, E., Elbrächter, M., 1999. Dinophyte chloroplasts and phylogeny - a review. Grana 38, 81–97.

Silva, E.S., 1962. Some observations on marine dinoflagellate cultures. II. *Glenodinium foliaceum* Stein and *Gonyaulax diacantha* (Meunier) Schiller. Bot. Mar. 3, 75–100.

Stamatakis, A., 2014. RAxML version 8: a tool for phylogenetic analysis and post-analysis of large phylogenies. Bioinformatics 30, 1312–1313.

Tillmann, U., Hoppenrath, M., Gottschling, M., Kusber, W.H., Elbrächter, M., 2017. Plate pattern clarification of *Heterocapsa triquetra* sensu Stein (Heterocapsaceae, Dinophyceae). J. Phycol. 53, 1305–1324.

Tillmann, U., Bantle, A., Krock, B., Elbrächter, M., Gottschling, M., 2021. Recommendations for epitypification of dinophytes exemplified by *Lingulodinium polyedra* and molecular phylogenetics of the Gonyaulacales based on curated rRNA sequence data. Harmful Algae 104, 101956.

Tillmann, U., Wietkamp, S., Kretschmann, J., Chacón, J., Gottschling, M., 2023. Spatial fragmentation in the distribution of diatom endosymbionts from the taxonomically clarified dinophyte *Kryptoperidinium triquetrum* (= *Kryptoperidinium foliaceum*, Peridiniales). Sci. Rep. 13, 8593.

Tippit, D.H., Pickett-Heaps, J.D., 1976. Apparent amitosis in the binucleate dinoflagellate *Peridinium balticum*. J. Cell Sci. 21, 273–289.

Tomas, R.N., Cox, E.R., Steidinger, K.A., 1973. *Peridinium balticum* (Levander) Lemmermann, an unusual dinoflagellate with a mesocaryotic and an eukaryotic nucleus. J. Phycol. 9, 91–98.

Trigueros, J.M., Ansotegui, A., Orive, E., 2000. Remarks on morphology and ecology of recurrent dinoflagellate species in the estuary of Urdaibai (Northern Spain). Bot. Mar. 43, 93–103.

Turki, S., Balti, N., Salah, Ben, C.-., 2007. First detection of *Kryptoperidinium foliaceum* (Stein 1883) in Tunesian waters. Harmful Algae News 35, 9–10.

Withers, N.W., Haxo, F.T., 1978. Isolation and characterization of carotenoid-rich lipid globules from *Peridinium foliaceum*. Plant Physiol. 62, 36–39.

Wolny, J.L., Kempton, J.W., Lewitus, A.J., 2004. Taxonomic re-evaluation of a South Carolina "red-tide" dinoflagellate indicates placement in the genus *Kryptoperidinium*. In Steidinger, K., Landsberg, J., Tomas, C., Vargo, G.A., (eds) Harmful Algae. Florida Fish and Wildlife Conservation Commission, Florida Institute of Oceanography, and Intergovernmental Oceanographic Commission of UNESCO, St. Petersburg, pp 443-445.

Wolny, J.L., McCollough, C.B., Rosales, D.S., Pitula, J.S., 2022. Harmful algal bloom species in the St. Martin River: surveying the headwaters of northern Maryland's coastal bays. J. Coast. Res. 38, 86–98.

Yamada, N., Bolton, J.J., Trobajo, R., Mann, D.G., Dabek, P., Witkowski, A., Onuma, R., Horiguchi, T., Kroth, P.G., 2019. Discovery of a kleptoplastic dinotom` dinoflagellate and the unique nuclear dynamics of converting kleptoplastids to permanent plastids. Sci. Rep. 9, 10474.

Yamada, N., Sakai, H., Onuma, R., Kroth, P.G., Horiguchi, T., 2020. Five non-motile dinotom dinoflagellates of the genus *Dinothrix*. Front. Plant Sci. 11, 591050.

Yoon, H.S., Hackett, J.D., Van Dolah, F.D., Nosenko, T., Lidie, K.L., Bhattacharya, D., 2005. Tertiary endosymbiosis driven genome evolution in dinoflagellate algae. Mol. Biol. Evol. 22, 1299–1308.

Zapata, M., Frage, S., Rodriguez, F., Garrido, J.L., 2012. Pigment-based chloroplast types in dinoflagellates. Mar. Ecol. Prog. Ser. 465, 33–52.

Žerdoner Čalasan, A., Kretschmann, J., Gottschling, M., 2018. Absence of co-phylogeny indicates repeated diatom capture in dinophytes hosting a tertiary endosymbiont. Org. Divers. Evol. 18, 29–38.

Žerdoner Čalasan, A., Kretschmann, J., Gottschling, M., 2019. They are young, and they are many: Dating freshwater lineages in unicellular dinophytes. Environ. Microbiol. 21, 4125–4135.

Zhang, Q., Liu, G., Hu, Z., 2011. Morphological differences and molecular phylogeny of freshwater blooming species, *Peridiniopsis* spp. (Dinophyceae) from China. Eur. J. Protistol. 47, 149–160.